Assessing the Role of GPIb-IX-V Complex in Transmitting Platelet Cytoskeletal Forces

Shirin Feghhi

A dissertation
submitted in partial fulfillment of the
requirements for the degree of

Doctor of Philosophy

University of Washnigton

2015

Reading Committee

Nathan J. Sniadecki (Chair)

Jose A. Lopez

James J. Riley

Wendy Thomas

Program Authorized to Offer Degree:

Mechanical Engineering

University of Washington

Abstract

Assessing the Role of GPIb-IX-V Complex in Transmitting Platelet Cytoskeletal Forces

Shirin Feghhi

Chair of the Supervisory Committee:
Associate Professor Nathan Sniadecki
Mechanical Engineering

Platelets rapidly seal wounds in blood vessels, preventing blood loss. They bind to exposed vascular matrix at the wound site through a highly specialized surface receptor, the glycoprotein (GP) Ib-IX-V complex, which recognizes von Willebrand factor (VWF) in the matrix. This bond is unique in that it becomes more stable as force is applied to it, i.e. a "catch" bond. After attaching to the wound site, platelets generate cytoskeletal forces to compact and reinforce the hemostatic clot.

Here, we evaluated the role of the GPIb-IX-V complex in the transmission of these forces, using arrays of flexible nanoposts to measure the contractility of individual platelets on VWF. We found that a significant proportion of cytoskeletal forces were transmitted to VWF through GPIb-IX-V, an unexpected finding given the widely held notion that platelet forces are transmitted exclusively through integrins. In particular, the GPIbα subunit of GPIb-IX-V mediates this force transmission through its interaction with the A1 domain of VWF on the platelet exterior and by binding the cytoskeletal actin-binding protein filamin A in the interior. We then used Chinese hamster ovary (CHO) cells that express GPIb-IX complex to investigate the mechanism by which GPIb-IX-V transmits cytoskeletal forces. We found that, these forces are myosin-dependent and are required to

maintain cell attachment through the GPIb-IX-V complex. Using CHO cells that lacked the filamin A binding site, a cytoskeletal protein that links the complex to the actin cytoskeleton of the platelets, we found that, this complex plays a major role in mediating the cytoskeletal force transmission through the GPIb-IX-V complex. Thus, the GPIb-IX-V/VWF bond is able to transmit cytoskeletal force, and uses this force to strengthen the bond through a catch-bond mechanism. This finding expands our understanding of how cells attach to matrices, describing a new mechanism in which catch bonds can be supported by internal forces in the absence of external forces to reinforce attachment.

We further studied the role of GPIb-IX-V complex in supporting contractile forces of hemostatic clots that form under flow condition, using a microfluidic device. We embedded a multitude of block and micropost pairs at the bottom of the microfluidic channel to measure the contractile forces of hemostatic clots as they formed between the block and micropost at pathological shear rates. We found that, in addition to supporting the clot at the wound site, GPIb-IX-V complex plays a significant role in supporting the contractile forces of hemostatic clots.

Together these results identify the first example of a non-integrin receptor that is capable of transmitting forces in platelets.

TABLE OF CONTENTS

LIST OF FIGURES

LIST OF TABLES

ACKNOWLEDGEMENTS

I would like to make acknowledgements to Dr. Adam Munday for his involvement in the first and second aim of this work and in particular for making the recombinant proteins and CHO cell lines, and Dr. Lucas Ting for his involvement in the third aim of this work. I would also like to make acknowledgements to Wes Tooley for all his help with the first and second aim of this work, Shreya Rajsekar and Magena Fura for helping with the data analysis for the second aim and Carly Morgan for helping with the data analysis for the third aim.

I would like to thank:

My primary mentor Dr. Nathan Sniadecki, for trusting the 23-year old me and recruiting me for his lab, for his incredible support and patience along the way, for encouraging me to pursue my ideas.

My co-mentor Dr. Jose Lopez, for talking biology and medicine with an engineer, for inspiring and encouraging me to combine the two, for teaching me numerous things beyond science.

My father, for giving me the rare gift of security, for bringing me up with high standards, for teaching me the concept of wanting more out of life than just the regular, for supporting me every time that I wanted to try something new, for reminding me of my capabilities whenever life is hard, and most importantly for being a role model of always pushing the limits beyond what is expected.

My mother, for understanding me, for dedicating her life to raising me and my sister, for teaching us how to love others unconditionally and how to give, for providing us a loving nourishing environment to grow up in, for always laughing and taking it easy: balancing our seriousness, and most importantly for being a role model of a being giver, setting the goal of her life to help those in need.

My sister, for being who she is, for sharing her life with me and letting me be a part of it.

The rest of my family, for being a warm, safe and happy family who brought us all up with the rare combination of freedom and love, for letting us ruin their carpets and walls as we learned to paint or made arts and crafts, for kissing us and hugging us frequently: cultivating in us the deep sense of worthiness.

My friends, who were my family while away from home, for filling all the nights that were dark and empty with their bright presence, for being there to explore new things together, for being my patient teachers helping me add new dimensions to my life, for being shoulders to cry on and buddies to share joy and happiness with, for being willing to get out of their way for me and for loving me.

My labmates, for never being my colleague but always my friends and the ones that I trusted and relied on, for making the many late-night working nights fun and memorable, for tolerating me when I was stressed out or sad.

Mrs. Javaheri, my second grade teacher, for killing the shyness in me when I was eight, for constantly telling me that I can do it if I want to, for giving me the confidence to be me, for being patient with all my 8-year-old creative/strange ways of trying to tell her how much I love her!

The children at the Omid cancer care hospital, for helping me find my perspective, for showing me what matters and what does not, for laughing with me, crying with me, and for their pure love, for embedding the desire of wanting to improve the quality of life in the deepest part of me by exposing me to their never-ending pains.

Wanwisa Kisalang and Maria Hopper, for being there for me as I was going through this journey.

AIMS OVERVIEW

AIM 1 Assessing the role of GPIb-IX-V in transmitting cytoskeletal forces in platelets

1.1 Development of a Single Platelet Force Measurement Technique

A nano-scale force measurement technique was developed to measure the contractile forces of single platelets. This tool was tested by measuring the forces of individual platelets on nanopost arrays that were coated with VWF.

1.2 Determining the Role of Integrin $\alpha_{IIb}\beta_3$ and GPIb-IX-V in Transmitting Cytoskeletal Forces in Platelets

Blocking antibodies against GPIb-IX-V complex and integrin $\alpha_{IIb}\beta_3$ were used to identify the role of each of the two receptors in transmitting cytoskeletal forces on nanoposts coated with VWF. In addition a recombinant protein was synthesized and used to block the A1 domain of VWF against GPIb-IX-V binding to further assess the contribution of this complex in force transmission. These findings were confirmed by using the recombinant A1 domain as a coating on the nanoposts.

1.3 Examining The Role of Cytoskeletal Force Transmission of GPIb-IX-V in Platelet Adhesion to VWF

To assess the role of GPIb-IX-V-transmitted forces in platelet adhesion, a molecular inhibitor, blebbistatin, against myosin motor activity was used to inhibit myosin ATPase activity and therefore cytoskeletal forces of platelets adhered to flat surfaces coated with the recombinant A1 domain. Platelet adhesion strength was tested by shearing the platelets off the surface, and quantifying the number of adhered ones.

AIM 2 Examining The Mechanism of GPIb-IX-V Force Transmission Using Chinese Hamster Ovary Cells

2.1 Examining the Role of GPIb-IX Complex in Transmitting Cytoskeletal Forces on A1 domain Compared to VWF

CHO cells expressing GPIb-IX complex, CHOαβIX cells, were used to further examine the capability of GPIb-IX-V complex in transmitting cytoskeletal forces. Micropost ar-

rays coated with either recombinant A1 domain or VWF were used to measure the forces generated by CHOαβIX cells and transmitted by GPIb-IX-V complex. CHOβIX cells were used to confirm that force transmission is through the GPIbα subunit.

2.2 Examining The Role of Filamin A and Myosin In The Forces that Are Transmitted through GPIb-IX-V

Three CHO cell lines containing, wild type GPIbα, GPIbα truncated at the 534th residue on the cytoplasmic tail, and GPIbα with F568A and a W570A mutations, were used to study the role of filamin binding in transmitting cytoskeletal forces. The latter two cell lines are unable to bind to filamin.

To test the role of myosin, blebbistatin was used to inhibit myosin ATPase activity. Micropost arrays coated with VWF were used for these assays.

AIM 3 Determining the Role of Integrin $\alpha_{IIb}\beta_3$ and GPIb-IX-V Complex in Transmitting Cytoskeletal Forces in hemostatic clots

A microfluidic device was developed to measure the contractile forces of hemostatic clots under shear flow condition. Blocking antibodies against GPIb-IX-V complex and integrin $\alpha_{IIb}\beta_3$ were used to identify the contribution of each of these receptors in transmitting the contractile forces of hemostatic clots.

INTRODUCTION

i) Biological Background

Overview on Platelets

Platelets are the smallest blood cells that are found only in mammals. They are fragmented from the cytoplasm of megakaryocytes and typically live between 7-10 days in the blood stream [1]. In an inactivated state, they are 2-4 μm discoid cells that circulate in the blood stream. Platelets get transported towards the vessel walls as they interact with other blood cells [2]. This placement allows them to rapidly carry out their primary function, which is to stop the bleeding in an event of a ruptured vessel wall in a process called hemostasis [3].

Platelet Biology

Overview

In an event of vascular injury, platelets are exposed to the collagen and surface bound von Willebrand factor (VWF). The VWF is either anchored to the endothelial cells or bound to collagen as well as soluble factors released in the blood [4]. This exposure rapidly activates platelets and helps them roll on the vessel wall. Platelets then further activate and change shape as they roll [5-7]. During this shape change, platelets go from discoid platelets to spiky spherical ones and ultimately to fully spread platelets, which resemble a fried egg shape (Fig. 1a-b).

During the process of shape-change, platelets increase their surface area by multiple folds, which allows them to cover the exposed subendothelium layer and release their granule content [8]. In their granules, they have multiple platelet agonists such as fibrinogen and ADP that further activate the platelets that are in their close vicinity. This activation then leads to the recruitment of more platelets that bind to the existing platelets using soluble proteins such as fibrinogen and VWF as multivalent bridges [9]. As the integrin receptors on the platelet plasma membrane get activated, platelets adhere to extra cellular matrices that contain an RGD domain such as fibrinogen, which then stabilizes their adhesion [10, 11].

Platelets are active contractile machineries that generate and transmit cytoskeletal forces [12, 13]. These forces are important in every step of hemostasis. Platelet forces reinforce and stabilize platelet-subendothelium adhesions as they bind to the wound site [13]. As a hemostatic clot forms, platelets use their contractile forces to compact the structure of the clot and close the gaps between platelets. This maintains a higher concentration of granule-released agonists within the clot [14]. Ultimately, platelets lower the risk of embolization by reducing the size of the clot as they pull on the fibrin strands within the (Fig. 1c) [15-17].

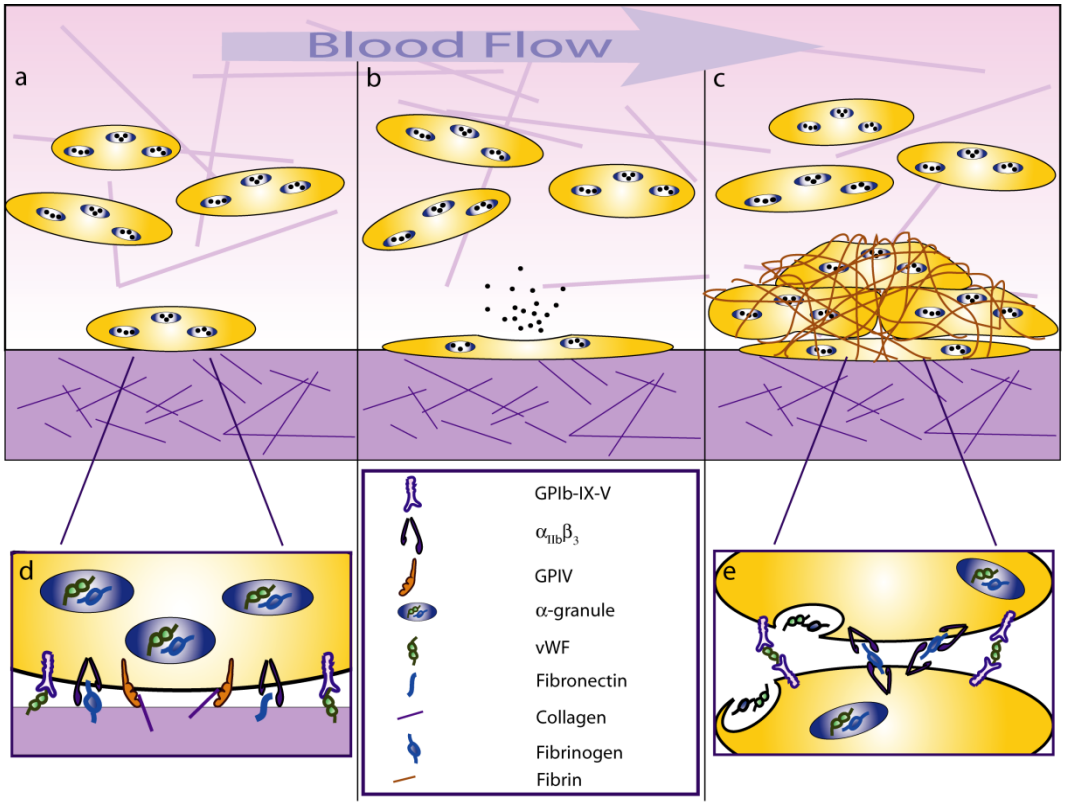

Figure 1 | Platelet Adhesion and Aggregation. **a**, Platelets adhere to the vessel wall when exposed to matrix proteins. **b**, Adhered platelets undergo shape change and release soluble adhesive proteins from their granules. **c**, A hemostatic clot is formed when platelets adhere to fibrin and each other. Specific receptor-ligand bonds mediate, **d**, platelet adhesion and, **e**, platelet aggregation.

Platelet Cytoskeleton

The platelet cytoskeleton allows platelets to maintain their discoid shape when exposed to hemodynamic shear forces [18]. It also helps maintain the structure of newly activated platelets once they are bound to the surface. Critical components of the platelet cytoskeleton include a spectrin-based membrane skeleton, a microtubule coil that is around the perimeter of the resting platelet, and a network of actin fibers [1]. Actin fibers are involved in the organization of platelet shape and structure in two major ways. First, actin monomers polymerize and depolymerize, and second motor protein myosin II binds to actin fibers and slides them past each other. Both of these mechanisms can move the platelet membrane in the form of pulling or pushing and cause a change in the structure [19, 20].

Actin is the most abundant protein in platelets with over 2,000,000 copies per platelet [21]. In resting platelets, around 800,000 of these copies polymerize to form about 2000-5000 actin fibers. The fibers are cross-linked at multiple points via proteins such as filamin and α-actinin and form a solid actin-based cytoskeleton [22, 23]. The shape change process in platelets is governed by actin fibers disassembling and reassembling in a different direction. As the platelet spreads, the granules and organelles translocate to the center of the platelet forming a fried egg shape [21].

Platelets form stress fibers to generate contractile forces and pull on the substrate at the sites of adhesion [24, 25]. Platelet activation leads to the activation of the most abundant integrin in platelet, $\alpha_{IIb}\beta_3$, which is linked to the actin cytoskeleton with a number of intermediate adhesion proteins. Examples of adhesion proteins in platelets include talin, vinculin, filamin, paxilin, zyxin, and α-actinin [22, 26-29]. These proteins are assembled in focal adhesion-like structures by kinases such as focal adhesion kinases and src. Contractile forces are then transmitted through integrin $\alpha_{IIb}\beta_3$ as motor protein myosin II moves along actin filaments and slides the anchored actin filaments past each other. Myosin II protein contains two heavy chains and two light chains, which get phosphorylated upon activation of myosin II and form small bipolar filaments [19, 30]. The phosphorylation leads to a conformational change in myosin, which allows for the engagement of the bipolar filaments on actin fibers and therefore, stress fiber formation. Myosin light chain can be phosphorylated both through myosin light chain kinase (MLCK) activity in a cal-

cium-dependent manner or by Rho kinase activity in a calcium-independent manner[31]. The forces generated as a result of myosin-activity are referred to as contractile forces or cytoskeletal forces in this thesis.

Platelet Receptors

Platelet receptors are involved in all platelet functions. This includes the initial adhesion of platelets to the wound site, platelet activation, platelet-platelet bridging by binding to soluble proteins or the fibrin mesh, and platelet contractile force transmission to the sub-endothelium or other platelets (Fig. 1d-e) [1]. Major platelet receptors belong to one of the following categories:

Integrins: Integrins are involved in platelet adhesion to their adhesive ligands and subsequent platelet signaling. An α-subunit and a β-subunit bind non-covalently together to form an integrin receptor [32]. Integrins usually have a high affinity state where they bind to their corresponding ligands rapidly and a low affinity state where they do not bind. They often go from a low affinity to a high affinity state upon activation via cytoplasmic signaling (inside-out signaling). Members of three families of integrins, β_1, β_2, and β_3, are present on platelet membrane, e.g. $\alpha_{IIb}\beta_3$, $\alpha_v\beta_3$, $\alpha_2\beta_1$, and $\alpha_v\beta_1$ [33]. Integrin $\alpha_{IIb}\beta_3$ is the most common receptor in platelets with 80,000-100,000 copies per platelet.

Leucine-Rich Repeat (LRR) Family: The LRR family of receptors is composed of 20–30 amino acids that are repeated in the structure and have an abundant amount of amino acid leucine [34, 35]. As these structures fold together, they form a protein domain called leucine-rich repeat domain. LRR receptors contain one or more of these domains. The most common LRR receptor on platelets is the glycoprotein (GP) Ib-IX-V complex with an average of approximately 50,000 copies of GPIb-IX-V complex per platelet [34, 35].

Transmembrane receptors: These receptors are the major agonist receptors on platelet membrane. Examples of these receptors include: thrombin receptors (protease activation receptor), ADP receptors ($P2Y_1$ and $P2Y_{12}$), serotonin, and dopamine receptors [36, 37].

Immunoglobulin Superfamily: The most famous receptor from this family present on platelets is GPVI, which binds to collagen and activates platelets [38, 39]. This receptor is considered both an adhesion receptor as well as a signaling receptor.

Each of these receptors plays multiple roles in platelets and has been widely studied. This thesis is particularly focused on integrin $\alpha_{IIb}\beta_3$ and GPIb-IX-V complex. These are the two most common platelet receptors and are also the two receptors that bind to VWF at sites of injury. Therefore, the next two sections discuss these receptors in more detail.

Integrin $\alpha_{IIb}\beta_3$

Integrin $\alpha_{IIb}\beta_3$ is a platelet-specific receptor that is present both on platelet membrane and in α-granules and is exposed as platelets spread [1, 9, 11]. This receptor is a heterodimer with a 1:1 ratio of α-and a β-subunits. Each of the subunits has a large extracellular domain and a short cytoplasmic tail. Integrin $\alpha_{IIb}\beta_3$ can bind multiple ligands since it recognizes the Arg-Gly-Asp (RGD) peptide sequence; therefore, any ligand containing this sequence is recognized by this receptor. The RGD sequence is present on both fibrinogen (fibrin) and VWF. Based on the conformation of α_{IIb} and β_3, the complex exists in two different conformations: i) bent state (low ligand-binding affinity) and ii) upright state (high ligand-binding affinity). It is widely held that upon activation, the change from bent to upright state happens as the headpiece moves away from the membrane, thus opening the headpiece for ligands to access their binding sites.

GPIb-IX-V Complex

GPIb-IX-V complex is responsible for 85% of the total linkages between the actin cytoskeleton and plasma membrane [1]. This linkage is mediated by an intermediate protein called filamin A [40]. GPIb-IX-V complex is an obvious candidate to stabilize the adhesion and aggregation of platelets because it is abundant on the surface of a platelet and it associates with the cytoskeleton [35, 41]. This complex is composed of four polypeptides — GPIbα, GPIbβ, GPIX, and GPV — in a 2:4:2:1 stoichiometry. GPIbα contains a binding site for the A1 domain of VWF in its extracellular domain and another binding site for filamin A in its cytoplasmic domain. Filamin A mediates the association of GPIb-IX-V with actin fibers in the platelet cytoskeleton, which further links the membrane to the

cytoskeleton [42]. The bond between GPIbα and the A1 domain is regarded as a catch bond, *i.e.* bond lifetime increases as force is applied to the bond [5, 43].

A number of other functions have also been described for GPIb-IX-V complex including:

- Containing binding sites for thrombospondin-1, thrombin, factor XI, factor XII and P-selectin
- Acting as a signaling receptor activating $\alpha_{IIb}\beta_3$ and $\alpha_2\beta_1$, upon binding to VWF, leading to the formation of a stable aggregate
- Linking actin cytoskeleton to the membrane

Filamin A

Filamins are scaffold proteins that link actin fibers to form a network of actin and stress fibers [42]. In particular, filamin A is the abundant form of filamin present in platelets that links the actin cytoskeleton of the platelet to the membrane and is also involved in the outside-in signaling upon binding of GPIb-IX-V complex to VWF. This binding rapidly activates platelets and consequently leads to inside-out activation of integrin $\alpha_{IIb}\beta_3$. The primary binding site for filamin A may be within residues 557-575 [44]. Blocking this binding site results in reduced binding of filamin A.

Role of Platelets in Hemostasis

The process of cessation of bleeding in an event of vascular injury is referred to as hemostasis [45]. Hemostasis involves a complex systemic response from the body, which involves multiple cellular and biochemical players. The main systems involved in hemostatic response are the coagulation system, the cardiovascular system, and the platelets and fibrinolytic system. During a healthy response to an injury, hemostatic clots form to prevent bleeding and allow for tissue repair. They then dissolve in a fibrinolytic process to allow for normal blood flow in the vessel. The balance between the two steps is critical because if the clot does not dissolve, it can lead to a pathological condition called thrombosis. On the other hand, if it dissolves prior to tissue repair, it can lead to hemorrhage, which is the reoccurrence of bleeding.

Hemostatic response can be broken down to primary hemostasis and secondary hemostasis [45]. Primary hemostasis refers to the initial response of endothelial cells at the site of injury as well as platelets circulating in the blood flow. This response includes secretion of VWF from endothelial cells, which allows for binding of circulating platelets. Platelets play a central role in primary hemostasis. Initially, they bind to the VWF secreted from endothelial cells and the VWF and collagen present at the wound site. This rapidly activates the platelet, which leads to their aggregation and the formation of the initial platelet-rich hemostatic clot. During this process, platelet aggregation is affected by a number of biochemical agonists such as ADP and soluble fibrinogen. The secondary hemostasis is centered on the response of the coagulation system, which lags behind the primary hemostasis. The secondary hemostasis involves a number of coagulation factors such as factor VIII, X, and XII, and leads to the formation of a fibrin mesh, which reinforces the platelet clot. These clots then dissolve away as plasmin digests the fibrin in the clot in a process called fibrinolysis. The focus of this work is on the role of platelets in primary hemostasis.

Role of Platelets in Blood Disorders Related to VWF-GPIb-IX-V Interactions

Thrombosis

Thrombosis is the formation of a thrombus at sites of reduced blood flow, injured vessel wall, or other hypercoagulable states [1]. Thrombosis can lead to partial obstruction of blood vessels or free-floating thrombus in the blood stream and cause vessel blockage and therefore tissue starvation. Thrombus is usually categorized based on its location and clinical signs. Examples include jugular venous thrombosis and pulmonary arterial thrombosis.

Glanzmann Thrombasthenia

Glanzmann thrombasthenia (GT) is the most common platelet disorder, where platelet aggregation fails because of the lack or non-functional presence of $\alpha_{IIb}\beta_3$ receptors on platelet membrane [46-48]. One out of every three GT patient suffers from regular mucocutaneous bleedings. This disease is often diagnosed by the lack of platelet aggregation in response to all platelet agonists. This failure in aggregation could be related to a mutation in the β_3 subunit of the $\alpha_{IIb}\beta_3$ receptor, which interrupts its normal interaction with solu-

ble fibrinogen. However, GT platelets have a normal ristocetin-induced response to VWF.

Bernard-Soulier Syndrome

Bernard-Soulier syndrome (BSS) is the second most common platelet disorder related to platelet receptors and cytoskeleton [47, 49]. BSS patients have prolonged bleeding times and suffer from thrombocytopenia. Their platelets are abnormally large and sometimes reach a size of 20 μm in diameter. GPIb-IX-V complex is not expressed on the platelet membrane of BSS patients, and all three functional subunits of GPIb-IX-V complex (GPIbα, GPIbβ, and GPIX) have mutations that prevent the normal expression of this complex. Since GPIb-IX-V links actin cytoskeleton to the plasma membrane, the loss of this receptor leads to the formation of more fragile platelets.

ii) Technical Background [1]

Techniques to Study the Role of Fluid Flow and Platelet Retraction Forces at the Micro- and Nano-Scale

A multitude of engineered devices have been developed to study clot formation at different stages and under different conditions such as high or low shear forces or in the presence of different agonists and antagonists [10, 50-55]. Amongst these technologies, micro- and nano-scale tools have been recently used to study platelet biology and thrombus formation dynamics [54, 56, 57]. One notable advantage of these tools over the conventional methods is that platelets and their adhesion receptors are micro- and nano-scale in size, so devices that are in the same size range as platelets can be used as programmable materials, in which the physical and adhesive interactions between platelets and their surroundings can be controlled and measured.

Platelet-Shear Flow Interactions

Early studies on platelet adhesion and aggregation were conducted in the absence of shear flow [58-60]. Soluble factors were assumed to be the main mechanism driving hemostasis, and shear flow was thought to have a minor effect. These studies on platelets

[1] Adopted from Feghhi et al. 2011

under static conditions examined the effect of different ECM proteins and biomaterials on platelet adhesion, shape change, and spreading, and the role of different agonists and inhibitors on platelet aggregation [60, 61]. These studies were helpful in gaining a better understanding of the process, but shear forces were later recognized as having a more fundamental role in platelet adhesion and aggregation process, rather than simply transporting platelets to the vessel wall through collisions with red blood cells [62-64]. Moreover, many of the findings from the static assays were found to be different under shear flow conditions, including biocompatibility of some of the materials used for stents, heart-valves and grafts [65].

Shear forces are produced by the fluid layers of blood passing by each other at different velocities and therefore applying a shearing force on particles in the flow. Shear rate is used to describe this gradient of velocities within a flow. Typically, shear rates are low in large vessels (<600 s^{-1}) and are high in the vessels with smaller diameters (up to 5000 s^{-1}). Depending on the shear rate, different platelet receptors can dominate the adhesive interaction with the vessel wall or other platelets. For example, $\alpha_{IIb}\beta_3$ strongly affects adhesion under low shear rate (<1000 s^{-1}), while GPIb-IX-V dominates under high shear rates (>10,000 s^{-1}) [6]. Therefore, to better understand platelet adhesion and aggregation, a number of perfusion chambers have been developed for *ex vivo* and *in vitro* studies (Fig. 2) [66]. These chambers can be configured to mimic the flow velocities and rheological properties of blood flow in an experimental setting, enabling one to study a range of shear forces and shear rates that platelets experience *in vivo*. Surface modifications such as different ECM coatings are possible and easy access to the chamber is provided, which can be advantageous for introducing different chemicals such as agonists and inhibitors into the flow.

Conventional Devices

Annular flow chambers were an early design used to study platelet adhesion as well as thrombus formation under *ex vivo* flow conditions (Fig. 2a,b) [67-69]. A segment of human or rabbit vessel was turned inside-out and fixed to a rod in the middle of a larger cylinder. Whole blood could be pumped through the cylinder to study platelet and fibrin deposition. The benefit of using the annular chamber was that it allowed for a large range

of control over the shear rate, which helped to identify the importance of VWF-GPIb-IX-V and fibrinogen-$\alpha_{IIb}\beta_3$ interactions under higher shear rates [49, 70-72]. The downside, however, was that since the adhesive wall was a vessel segment, platelets were exposed to the native ECM, which had an uncharacterized composition of ligands with which the platelets could interact, making it difficult to study specific receptor-ligand interactions.

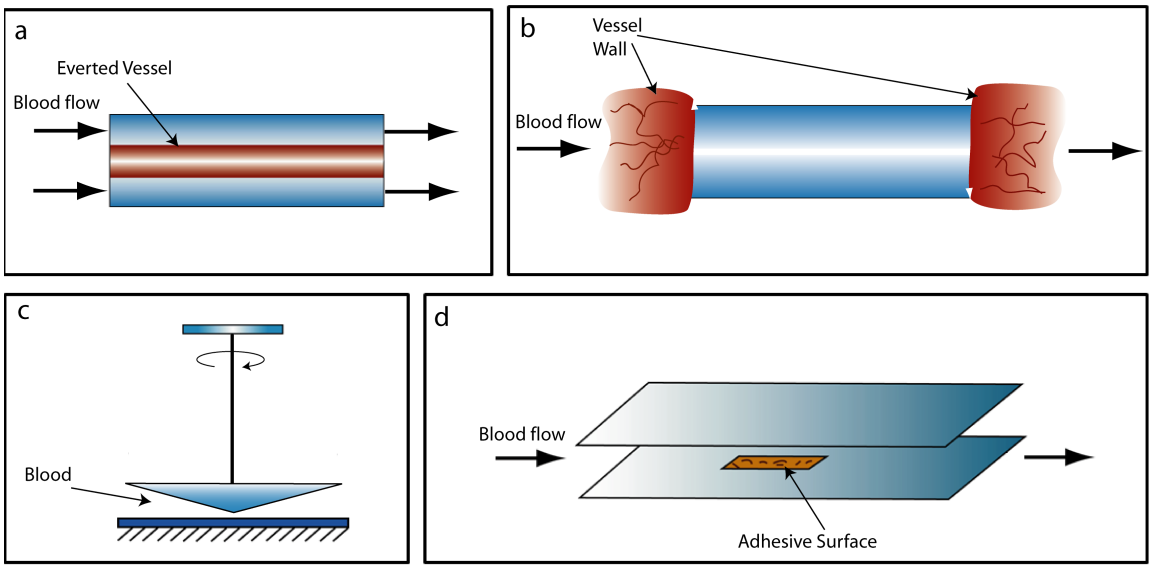

Figure 2 | Conventional Flow Devices: **a**, Annular flow chamber, **b**, Tubular flow chamber, **c**, Cone and plate flow device, and **d**, Parallel plate flow chamber.

Tubular flow chambers allowed for better control over the adhesive interactions, but it did not have the same control over the shear rate as a result of the *ex vivo* nature of the assay. The typical setting of these assays consists of a tube coated with the targeted ECM or anticoagulant and surgically inserted between an artery and vein to form a shunt. This approach allowed for studies on platelet binding to surfaces with well-defined ECMs [73]. In addition, the tubular devices were helpful in studying drug effects on platelets due to the usage of blood in the absence of anticoagulants. Different synthetic graft and stent materials could be examined using these devices because of the particular bio-compatibility issues that they can introduce when exposed to the blood and the potential for clot formation possibly leading to restenosis, embolism, or other secondary defects [74-76].

Cone and plate flow devices are another type of device used to expose platelets to uniform and well-defined shear rates (Fig. 2c) [68, 77]. To run the assay, a sample of blood or platelet-rich plasma is placed between a rotating cone and a stationary well, which exposes the sample to the shear rate that is determined by the rotation speed and the angle of the cone [78, 79]. Cone and plate flow devices have been used to investigate platelet adhesion and aggregation on different ECMs [80-82]. More recently, these devices have been used to produce more complicated flow regimes, such as pulsatile shear stresses that mimic stenosed regions or recirculation zones [83]. Moreover, these devices have been combined with an upright epi-fluorescence microscope to allow for real-time studies of the thrombogenecy of biomaterials [84]. One shortcoming of this assay is that the open surface at the rotating cone can lead to evaporation of the sample.

Parallel plate flow chamber is used most frequently among the types of flow perfusion systems (Fig. 2d) [85, 86]. The early design was a channel with a cover-glass holder at the bottom where different ECMs could be introduced to the system using a cover-glass that was pre-treated with adhesive proteins. After exposure to flowing platelets or whole blood, the cover-glass could be removed, fixed, stained, and analyzed for the platelet adhesion and thrombus formation [87]. Later with the usage of new imaging techniques, channels were made of clear and thinner materials to allow for a microscope to be close enough for live-microscopy studies of platelet adhesion and thrombus formation [52, 88]. An advantage of parallel plate flow chambers over the other devices is that they can be modified to mimic different *in vivo* conditions; among these, pulsatile flow [89] and disturbed flow [90] can be generated with slight modifications to the pumping system or flow chamber design. Porous membranes can also be used instead of cover-glass to allow for controlled introduction of chemicals to the system through the membrane [91]. These membranes help mimic the release of different chemicals from endothelial cells such as agonists and anticoagulants. One limitation with parallel plate flow chambers is the use of anti-coagulated blood in these studies. To overcome this limitation, these chambers have also been used *ex vivo* by surgically inserting them into the subject's body to study the thrombogenic characteristics of grafts and stents [92]. Parallel plate flow chambers have been very successful in determining many of the unknowns in platelet adhesion and ag-

gregate formation, including the effect of shear on platelet-ECM binding mechanisms as well as clot formation and stability [4, 9, 51, 52, 88, 93, 94].

Microfluidic Devices

Miniaturized versions of parallel plate flow chambers have been developed to improve the micro-and nano-scale capabilities for studying platelets under shear flow [95, 96]. These microfluidic devices are typically made of a silicone rubber (polydimethylsiloxane, PDMS), which can be casted against a silicon master to replicate its features [97]. This process is referred to as soft lithography and allows for high precision in replicating micro- and nano-scale features that have been built onto a master silicon wafer using processing tools for semiconductor fabrication [98]. To build the microfluidic devices, multiple layers of PDMS are bonded together, where each layer contains a part of the design of channels and posts [99]. This method is quite versatile and a variety of unique and creative chamber configurations have been achieved.

Microfluidic devices have been used in biological studies because they have the capability to mimic the *in vivo* conditions closely. They have been used effectively in vascular research studies, e.g., shear flow mechanotransduction, cell-cell interactions, cell migration, and targeted drug delivery [100, 101]. In particular, they have been used to confirm the observations made using conventional flow devices, but at the same time, they provide powerful insights into the interactions between platelet receptors and matrix ligands under different shear rates [9, 102, 103]. Additionally, they have been used to study clot formation and the role of different agonists [104], anticoagulants [105], and strain microcirculation zones [106] (Fig. 3).

These devices have been able to successfully resolve one of the major short comings of conventional flow chambers, which is the high volume consumption of sample blood and reagents. Human subjects provide adequate volumes of sample blood to run assays using parallel plate flow chambers, but in some cases, a sample volume of blood is limited, e.g., sickle cell anemia. Blood from mice, which is advantageous for studying genetic modification, has major limitations in sample volume since an average-sized adult mouse can yield less than 1 mL of blood volume [107]. In comparison, microfluidic devices require lower volumes of sample blood, usually less than 50 μL [104, 108-110]. The lower volumes

possible with microfluidics have expanded the studies on platelets from knock-out mice, which in turn have provided more insights on the role of platelet receptors in adhesion and aggregation [110, 111].

Microfluidic devices have also been helpful in running assays at different shear rates [112]. A variety of environments can be introduced under these shear rates, using patterning techniques to create wound-like environments with well-defined areas of adhesive protein (Fig. 3a) [108]. They have enabled studies on aggregate formation to be run with multiple experiments simultaneously (Fig. 3b) [105, 113] or with controlled concentration of agonists (Fig. 3c) [104]. Of particular note, a novel microfluidic device has been used to investigate aggregate formation after exposure to micro-gradients in different shear rates (Fig. 3d) [54, 106]. In these studies, the walls of the microchannel were built with a section that narrowed and then expanded in width as the flow passed over an obstruction in the channel. This configuration was used to generate a gradient in the shear rate that was similar to what platelets experience as they pass through a stenosis *in vivo*. Changes in the shear rate were able to initiate platelet adhesion and aggregation, even when the platelet response to conventional agonists was blocked. The implications of these studies suggest that biomechanical factors can activate platelets independent of biochemical factors.

Finally, microfluidic devices have been used to run parallel assays under different conditions [105, 108, 113]. Since they work with very low blood volumes they can be used to run parallel experiments varying a parameter such as shear rate [108, 114], chemicals including inhibitors (Fig. 3e) [115], and matrix coatings [113]. The advantage of parallel microchannels is that they significantly reduce the overall assay time since all experiments can be conducted simultaneously. They also help to reduce the sample-to-sample variability and effects of other randomly introduced factors (such as operator handling) because the experiments are run at the same time in the same device. Therefore, microfluidic assays afford a higher degree of reliability in assessing platelet functions or aggregate formation assays when varying environment conditions.

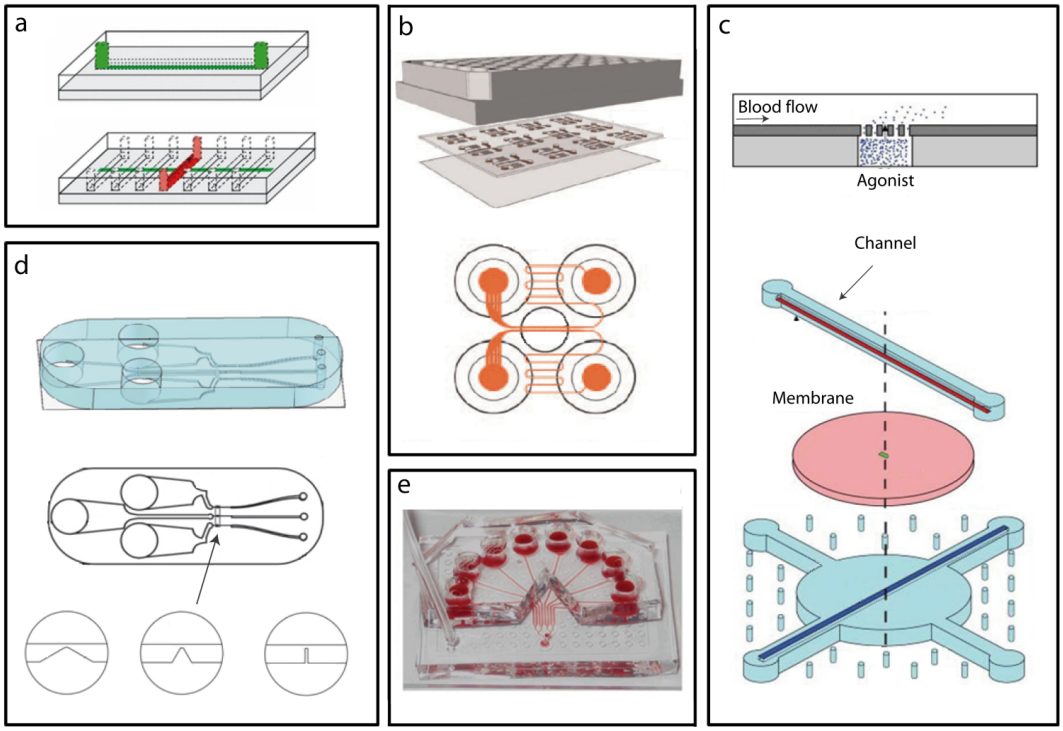

Figure 3 | Microfluidic Devices: **a**, A microfluidic device with seven parallel microchannels (red) to run simultaneous experiments under different shear rates. A horizontal channel (green) is used to flow ECM proteins in solution and deposit the protein as adhesive patches on the array of horizontal channels used for blood flow. Adapted with permissions from [108]. **b**, A compact array of microfluidic devices allows the operator to run multiple experiments simultaneously. Adapted with permissions from [113]. **c**, A microfluidic device used for the controlled release of agonist through a membrane structure at the bottom of the flow channel. Adapted with permissions from [104]. **d**, A microfluidic device with three different types of obstructive geometries in the main channel is used to examine the effect of gradients in the strain rate. Adapted with permissions from [106]. **e**, A microfluidic device used to expose the same sample of blood to different inhibitors. Adapted with permissions from [115].

Platelet Clot Retraction

Clot retraction is the final step in platelet aggregate formation. Platelets pull on fibrin strands to consolidate the size of the hemostatic clot to allow the flow of blood to re-commence. Consolidation of the clot reduces the fluid drag acting on it [15-17], but also leads to tighter association between platelets and fibrin strands that prevents fibrinolysis [14]. Moreover, actin-myosin force generation in platelets helps stabilize their receptor-ligand adhesions through integrin-related mechanotransduction [116]. To examine clot retraction, a number of conventional methods have been developed that are briefly discussed here (Fig. 4).

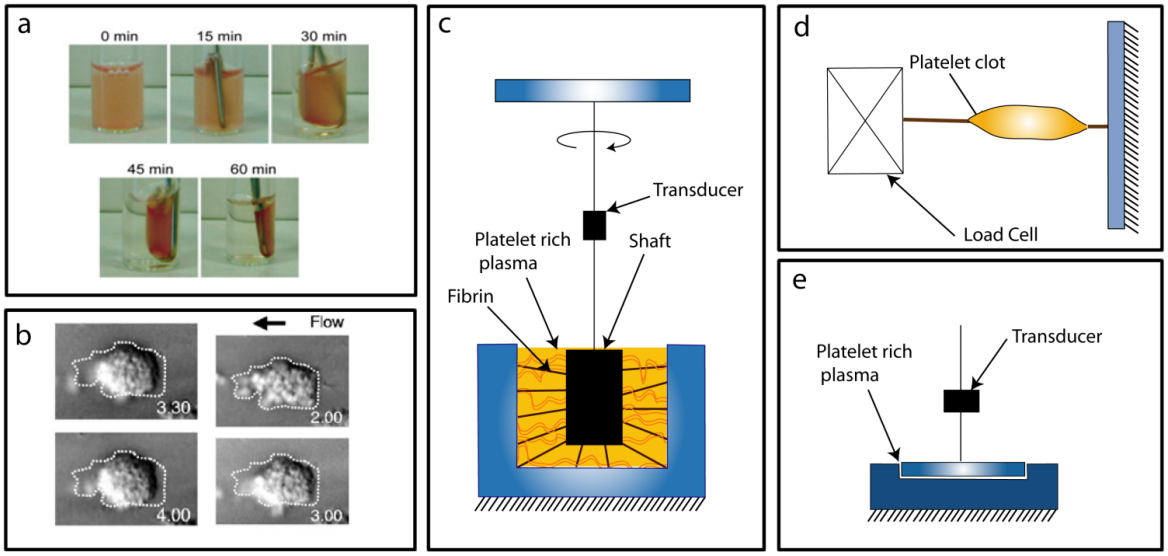

Figure 4 | Conventional Platelet Force Assays: **a**, Clot retraction assay. Adapted with permissions from [117]. **b**, *In-vitro* observations of thrombus consolidation. Adapted with permissions from [55], **c**, Thromboelastography, **d**, Clot strip assay, and **e**, Clot retractometry.

Conventional Force Assays

Clot retraction assay is a common method to assess consolidation by monitoring the volume change in a thrombus in vitro. This method is simple to implement because platelet-rich plasma is placed in a vial with a metal rod and agonists are added to initiate the thrombus formation (Fig. 4a). As the thrombus consolidates around the rod, plasma is extruded from its volume. The degree of retraction is determined by removing the thrombus from the vial and measuring the remaining plasma volume. This method has provided

useful insights into the important role of $\alpha_{IIb}\beta_3$ and its integrin-related kinases in clot retraction [117-119]. Recently, this method has been adapted for microscopic studies where the volume change of a micro-clot is monitored by tracking the movement of its platelets as they pull closer together (Fig. 4b) [55]. However, the general shortcoming of the clot retraction method is that it does not allow for the direct measurement of platelet forces, but merely the volume change associated with clot retraction.

Thromboelastography examines clot retraction by measuring the viscoelastic characteristics of blood during clot formation under low shear (Fig. 4c) [120-123]. The system consists of a stationary cup that holds the sample and is rotated back and forth by a small angle. A pin is suspended in the blood sample and is normally stationary, but when fibrin strands and platelet adhesions formed, the torque from the rotating cup is transferred to the pin, which then rotates. The strength of these fibrin strands and platelet force affects the motion of the pin. Its rotation is measured by a transducer and reported as the output of the system. Key information obtained by thromboelastography consists of the initiation of coagulation, propagation kinetics, fibrin-platelet interaction, clot firmness, and fibrinolysis [122]. The main shortcomings of this method, however, are its sensitivity to mechanical vibrations and long assay time in the absence of chemical agonists. To address these shortcomings, a variation of this method called rotating thromboelastography has been designed which transmits the pin signal through an optical detector and the movement is initiated by the pin [124]. This technique is considered a whole blood coagulation assay. It is used to predict surgical bleeding and as an aid to determine blood product usage for a patient clinically [120].

Platelet clot strips was the first technique to directly examine contractile forces within the clots (Fig. 4d). Clot strips are formed by pouring platelet-rich plasma into a cylindrical tube and activating them with thrombin or heating up the clots [125-127]. After removing the clot strip from the tube, one end is tied to a rigid support and the other is tied to a load cell which monitors the retraction force in the sample. This technique has been used to study the effect of different agonists on the tension generated in a clot [125], receptors involved in fibrin-platelet binding [128], and alignment of fibrin in the clot contraction [126]. The positive aspect of this method is that since the assays are done in a

fluid bath, it is possible to change the conditions of the experiment by changing the bath solution. Its shortcoming, however, is that the clot needs to be directly manipulated when it is mounted onto the load cell, resulting in mechanical disruption of the fibrin-platelet adhesions which can compromise the testing results.

Clot retractometry examines platelet clots by directly forming them between a cup and plate which is coupled to a strain gauge transducer with a voltage output (Fig. 4e) [129, 130]. The plate is in contact with the blood sample and during clotting, fibrin strands as well as platelet aggregates connect the cup and plate. Once clots are formed, platelet forces pull on the fibrin strands, which in turn pull down on the plate. This movement is then transferred to a load cells that reports the output of the system. The advantage of this method over others is that it allows for measurement of the force at the onset of clot formation and does not require additional physical handling of the growing clot. Clot retractometry has been used extensively to investigate the clinical relevance of platelet forces in cardiovascular disease and medical treatments [130-139].

Micro/Nano Force Assays

Conventional force measurement techniques discussed here have been successful in demonstrating the importance of platelet forces in hemostasis. There is, however, an inherent size and resolution limitation within these methods. Platelet cytoskeleton-fibrin interactions are nanoscale and complex with glycoprotein receptors playing different roles in adhesion, aggregation, and clot retraction. The macro-scale dimensions of the conventional techniques do not allow for microscopic imaging, which can help reveal the dynamic features of thrombus formation. Moreover, the fibrin meshwork has strain-stiffening behavior under load, which confounds the direct measurement of platelet forces. Therefore, researchers have begun to explore tools that come from micro- and nanoscale technologies in order to gain more insight into the mechanobiology of platelets.

Micropost arrays are a novel microscale force sensor that have been used previously to measure cellular traction forces [140, 141]. This sensor is an array of micro-size, flexible, vertical posts that bend in proportion to the forces that cells apply at tips of the posts. The posts are made from PDMS using soft lithography, similar to the fabrication of microfluidic devices. These arrays have been used to study cell migration [141], cell spreading

[140], and traction forces [140, 142-147]. Forces within monolayers [141, 148-151] as well as tissue constructs [152], and cell-cell forces [153, 154] have also been examined using this tool. At the same time a variety of cell studies have been done using different types of cells, such as fibroblasts [140, 145, 146, 155, 156], smooth muscle cells [140, 157], cardiomyocytes [158, 159], epithelial cells [144, 155], endothelial cells [157], and stem cells [143, 160]. Micropost arrays are considered a novel tool for cell mechanic studies because they can be used to map the traction forces of cells spread over multiple posts. Additionally, live studies are possible with microposts to investigate the dynamics of cytoskeletal force development. The unique property of this sensor is that it can be bio-functionalized with different adhesive proteins to study specific receptor-ligand interactions. Micropost arrays have been recently used to investigate platelet forces in more detail (Fig. 5a). The arrays have been used to examine the effect of thrombin concentration on contractile forces of platelet aggregates as well as the adhesive interactions with fibronectin and fibrinogen [56]. Comparisons also have been done between quasi-static and live imaging of aggregate formation to show its spatio-temporal capability in assessing platelet functionality and thrombus formation.

Atomic force microscopy (*AFM*) is another technique that is typically used for nano-scale characterization of materials, but it has been adapted to study the mechanical properties of cells and single molecules [161]. AFM uses a flexible tip that acts like a cantilever to measure forces in the vertical direction. The deflection of the tip is measured from a laser beam that is reflected off the back of the tip and towards an array of photodiode detectors. AFMs have been used to investigate cell mechanics and cytoskeletal elasticity [162-169] as well as cell-cell forces [170-172], receptor-ligand dynamic interactions [170, 173], and cytoskeletal proteins [28, 174]. Recently, AFM has been used to study the nature of the ligand-receptor bond between vWF and GPIbα in platelets. Platelet adhesion to the vessel wall likely involves catch-bonds between vWF and GPIbα because high shear stress leads to greater binding [175]. This observation is similar to the catch bond-like behavior in other integrin types where the strength of the bond increases with the applied external force [176, 177]. Using an AFM, the bond lifetime of a GPIbα-coated tip to a surface coating of vWF A1-domain was confirmed to have catch-bond behavior be-

cause the lifetime of the bond increased up to a peak load value and then reduced at higher loads as the catch-bond transitioned to a slip-bond [43].

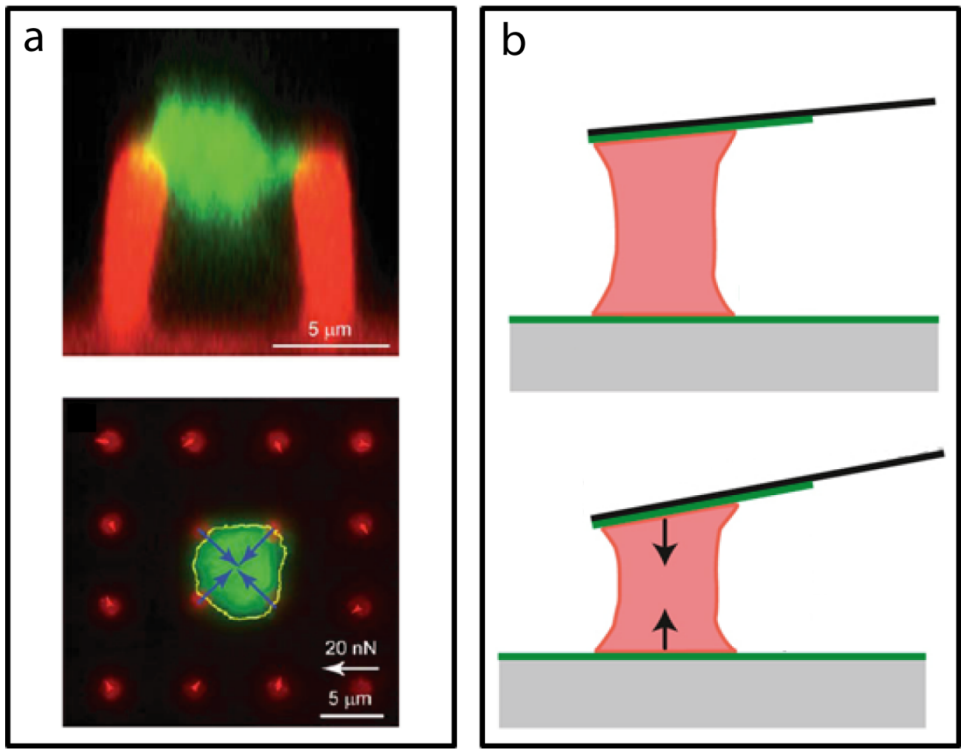

Figure 5 | Micro/Nano Platelet Force Assays: **a**, Micropost arrays. Top: side-view of a platelet clot (green: actin) on two microposts (red: DiI). Bottom: top-view of a platelet clot on four microposts within an array. Platelets produced contraction forces that bend the microposts (blue arrows). Adapted with permissions from [56]. **b**, Atomic force microscopy (AFM). Top: AFM tip is in the original position because the platelet attached to it has not contracted. Bottom: AFM tip is bent by the contraction force of the platelet. Adapted with permissions from [57].

Another significant study done using AFM was the direct measurement of retraction forces from a single platelet (Fig. 5b) [57]. The AFM tip was integrated with a fluorescence microscope and the tip was coated with fibrinogen. This technique was not only able to measure the contractile force of a single platelet, but it was also able to use AFM tips of different spring-constants to show that platelets regulate their retraction forces in proportion to the stiffness of the surrounding clot structure. These findings indicate that

clot stiffening happens through the contraction of platelets as well as the strain-stiffening of fibrin strands under the tension generated by platelet forces.

AIM 1: ASSESSING THE ROLE OF GPIb-IX-V IN TRANSMITTING CYTOSKELETAL FORCES IN PLATELETS

1.1 Development of a Single Platelet Force Measurement Technique

1.1 Background

Platelets play a central role both in hemostatic and thrombotic clots. One of these roles in the ability of platelets to generate cytoskeletal forces and transmit them to the neighboring platelets as well as the underlying matrix [116]. These forces then lead to the formation of a more stable and structurally compact clot that can hold on to the vessel wall and resist fluid forces, which would otherwise rupture it. Therefore, understanding the nature of these contractile forces as well as the mechanism with which they are transmitted to neighboring platelets and matrices is of great importance in understanding the clotting process.

A number of conventional assays exist that measure clot contractility in micro-clots or clot strips. These assays, as described in the previous chapter, include platelet aggregometry, cone and plate shearing, clot retraction assays and thromboelastography [125, 178, 179]. Aggregometry and clot retraction assay do not directly measure the contractile forces generated by platelets but rather measure the percent reduction in clot volume. Cone and plate shearing and thromboelastography measure the viscoelastic characteristics of clots and correlate the stiffness of the clot to the contractile forces of the platelets within the clot. Although these methods all lead to great insight in understanding the biology of clots, they have their limitations. More recently, microposts were used to measure the contractility of platelet micro-aggregates. Microposts directly measure contractile forces of platelet micro-aggregates and therefore isolate the role of platelets in clot contraction.

Investigating the role of GPIb-IX-V complex in transmitting cytoskeletal forces to VWF requires a method, which measures platelet contractile forces at single platelet level. These measurements are advantageous since they eliminate the role of other players in clot contractility such as platelet-platelet interaction and the effect of the concentration of soluble proteins and focuses on the ability of individual platelets in generating and transmit-

ting force. Single platelet forces were previously calculated by measuring the displacement of beads imbedded in polyacrylamide gels as platelets contract [180]. In addition, atomic force microscopy (AFM) has been previously used to measure single platelet forces by trapping platelets between an AFM tip and a glass slide coated with fibrinogen [57].

Here, using e-beam lithography we scaled down the micropost technology and developed an array of nanoposts. We functionalized the tips of the nanoposts with VWF and calculated single platelet forces by measuring the deflection of individual nanoposts. This approach consists of seeding platelets on silicone nanoposts, immunofluorescently staining and imaging them, and assessing their contractile properties using a custom written MATLAB code that analyzes the position of the tips of the nanoposts.

1.1.2 Methods

Force Sensor Design

A force sensor was specifically designed and fabricated to measure single platelet forces under various biological conditions and allow for immunofluorescent imaging of the platelets. This force sensor is replicable, which is favorable for comparisons between multiple replications of experiments.

Fabrication of the Nanopost Array Silicon Master

A silicon wafer was spin-coated with a 1.55 μm-thick layer of ma-N 2410 resist (Micro Resist Technology, GmbH, Berlin, Germany). The resist was patterned with circles that were 850 nm in diameter and 2 μm in center-to-center spacing using a JEOL JBX-6300FS e-beam lithography system (100 kV energy, 20 nA current). The resist was developed in MF-319 developer (Shipley Company, Marlborough, MA), and then etched with a fluorine-based inductively coupled plasma (ICP) process using an Oxford PlasmaLab 100 system to create a silicon master with an array of vertical cantilevers. Using scanning electron microscopy (SEM), we measured the dimensions of the silicon nanoposts in the array to be 850 nm in diameter, 2 μm in spacing, and 3.5 μm in height (Fig. 6a).

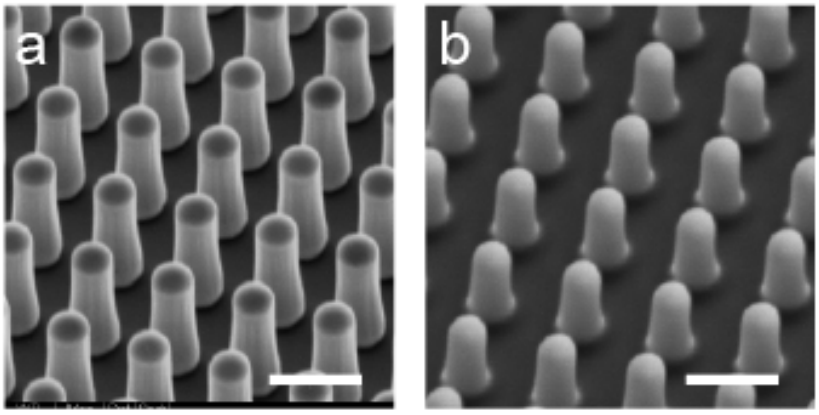

Figure 6 | SEM micrograph of, **a,** an array of silicon nanoposts, and, **b,** a PDMS replicate of the array. Scale bars are 2 μm.

Soft Lithography

A double-casting technique was used to replicate the features of the silicon master in polydimethylsiloxane (PDMS, Sylgard 184; Dow Corning, Midland, MI). Following a process that has been previously described for microposts [181], we made a negative mold by casting a 10:1 ratio of base-to-curing agent of PDMS from the silicon master and then passivating its surface with (tridecafluoro-1,1,2,2-tetrahyrooctyl)-1-trichlorosilane (United Chemical Technologies, Bristol, PA). We poured liquid PDMS into the negative molds, placed a clean glass slide on top of the liquid PDMS, and baked it at 110°C for 15 hours. Once the PDMS was cured and permanently bonded to the glass, we peeled it from the negative mold to create an array of PDMS nanoposts that were freestanding. We repeated the double-casting process to make new arrays of nanoposts for each experiment.

We noted that PDMS nanoposts did not replicate the exact dimensions of the original silicon master (Fig. 6b). Using SEM, we measured the dimensions of the PDMS nanoposts to be 850 nm in diameter (D), 2 μm in spacing, and 2.5 μm in height (L). These dimensions were consistent between nanoposts arrays that were replicated from the same master. For PDMS baked at 110°C for 15 hours, we measured the Young's modulus of PDMS (E) to be 3.2 MPa using tensile testing. In accordance with Euler-Bernoulli beam theory, the bending stiffness of the arrays was calculated to be $k = 3\pi ED^4/64L^3 = 15.7$ nN/μm (Fig. 7).

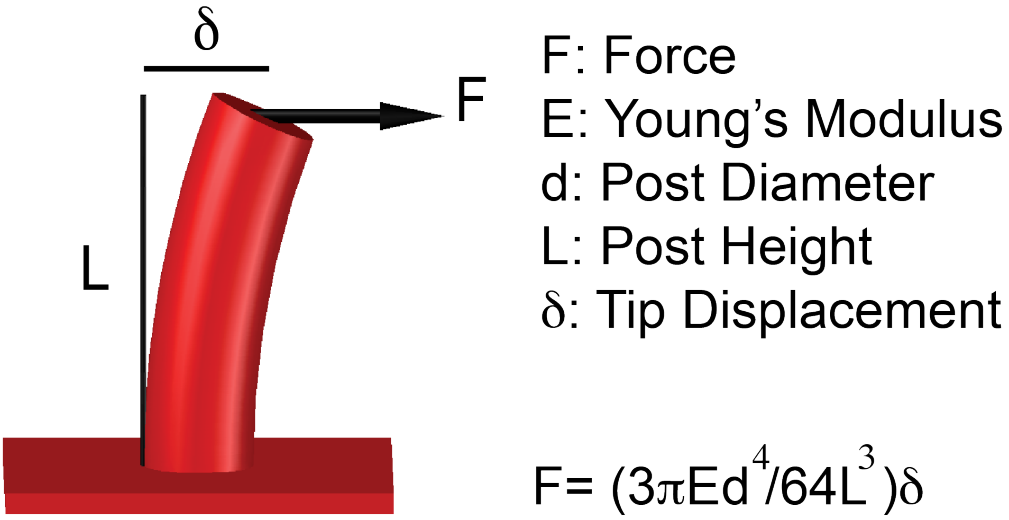

Figure 7 | The calculation of force on a nanopost by a platelet is based on the Young's modulus of PDMS (*E*) and the length (*L*), diameter (*D*), and deflection (δ) of the nanopost.

Coating Nanoposts with VWF

To coat the tips of the nanoposts, we placed a 300 µL droplet of VWF solution (10 µg/mL in PBS) on top of the nanopost arrays for 2 hours. The droplet of VWF solution stayed on the tips of the nanoposts and did not wet the sidewalls. We noted that the adsorbed VWF on the tips of the nanoposts created fiber-like strands between the tips of the nanoposts (Fig. 8).

After coating with VWF, we submerged the arrays of nanoposts in Alexa Fluor 594-conjugated bovine serum albumin (BSA) (20 µg/mL in PBS; Sigma, Bloomington, MN) for one hour. This treatment facilitated the fluorescent visualization of the nanoposts and blocked the adsorption of other proteins. For additional blocking, we submerged the arrays of nanoposts in a solution of 0.2% Pluronic F-127 in PBS (BASF Ludwigshafen, Germany) in PBS for one hour. The quality of the blocking layer was checked by incubating platelets with arrays of nanoposts treated with Alexa Fluor 594-conjugated BSA and Pluronic F-127, but with no VWF coating.

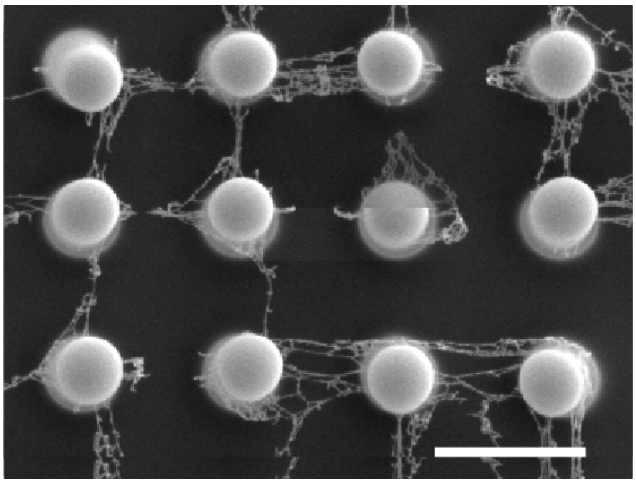

Figure 8 | SEM micrograph of VWF strands that formed on the tips of the PDMS nanoposts. Scale bar is 2 μm.

Blood Collection and Platelet Isolation

We collected whole blood from healthy donors in vacuum tubes with acid citrate dextrose solution (ACD; BD Medical, North Bend, WA) and performed our experiments within 1 hour of blood collection. We centrifuged whole blood samples at 120×g for 20 minutes to obtain platelet-rich plasma (PRP). We centrifuged the PRP at 1200×g for 10 minutes and removed the platelet-poor plasma. We washed the platelets that were pelleted by resuspending them in CGS washing buffer (120 mM NaCl, 13 mM sodium citrate, and 30 mM glucose at pH 7) and centrifuging again at 1200×g for 10 minutes. We then removed the supernatant and resuspended the pelleted platelets to the original PRP volume in Tyrode's buffer (10 mM HEPES, 138 mM NaCl, 5.5 mM glucose, 12 mM NaHCO3, 0.36 mM Na2HPO4, 2.9 mM KCl, 0.4 mM MgCl2 and 0.8 mM CaCl2, pH 7.5). All reagents for CGS and Tyrode's buffer were from Sigma (Bloomington, MN).

Experimental Protocol for Seeding Platelets onto Nanoposts

We added platelets in suspension to dishes containing arrays of nanoposts submerged in Tyrode's buffer. As they settled to the bottom of the dish, they encountered the tips of the nanoposts and adhered to the coatings of VWF. After 10 minutes of incubation with the sample of platelets, we gently washed the arrays of nanoposts in PBS to remove the unat-

tached platelets and incubated them in Tyrode's buffer for an additional 30 minutes to allow the platelets to spread and contract. We fixed the platelets on the arrays of nanoposts with 4% paraformaldehyde, permeablized them with 0.1% Triton X-100 (Sigma, Bloomington, MN) and stained with Alexa Fluor 488-conjugated phalloidin (Life Technologies, Carlsbad, CA) for 1 hour. After staining, the samples were mounted on glass slides with Fluoromount-G (VWR International, Radnor, PA) for confocal microscopy.

Scanning Electron Microscopy

Samples of platelets on nanoposts were dried using critical point drying techniques, as described previously 25. In brief, we dehydrated the samples by incubation in dishes of 50%, 70%, 80%, 90%, and 100% ethanol for 10 minutes each. A critical point drying system (CPD; Polaron E3100; Quorum, Houston, TX) was then used to dry the samples overnight to prevent damage to the platelets and nanoposts. Dried samples were given a conductive coating by sputtering with gold-palladium (60%-to-40%) for 90 seconds. The samples were imaged using a scanning electron microscope (SEM, FEI Sirion) with a voltage of 5 kV at a working distance of 10 mm. As others have noted, drying biological samples with CPD causes their structures to shrink. We observed shrinkage in our samples of platelets on nanoposts from CPD because the deflections of the nanoposts were substantially larger than the deflections observed using confocal microscopy.

Confocal Microscopy

To acquire images of the platelets and nanoposts, we used a confocal microscope (Zeiss LSM 510) equipped with a 63× oil objective (NA 1.42). A step size of 0.31 μm was used to construct a Z-stack of platelets and nanoposts. We then extracted the raw images for image analysis of the nanoposts and platelets.

Force and Spread Area Analysis

A manual code was developed in MATLAB to analyze the images of the samples obtained from confocal microscopy. The deflections of the nanoposts were determined by comparing the centroid of the nanoposts in the confocal images taken at the top and base of the nanoposts. We calculated the force vector at each nanoposts by multiplying the measured deflections by the bending stiffness of the nanoposts:

$$F_i = k\delta_i$$

where F_i is the force at a single nanopost at the i^{th} post, k is the bending stiffness of the post (15.7 nN/μm), and δ_i is its deflection at the i^{th} post. Assuming that each micropost can be modeled as a cantilever beam that is fixed at one end, and undergoes small deflections at the other, the stiffness can be calculated using beam bending theory [181]:

$$k = \frac{3\pi E d^4}{64L^3} \tag{3}$$

where d is the diameter (850 nm), E is the Young's Modulus (3.2 MPa), and L is the length (2.5 μm) of a nanoposts.

We calculated the total force per platelet by summing the magnitudes of the force vectors at each nanopost underneath a platelet. Spread area was quantified from the actin image using the outer edge of the cell on the posts.

Measurement Sensitivity

In order to quantify the minimum force measurements that were reliable, we analyzed a number of random empty regions of the nanopost arrays using our force analysis code. We found that any force reading about 1.1 nN per post is reliable.

1.1.3 Results

Our fabrication method using electron-beam lithography and inductively coupled plasma etching successfully resulted in arrays of silicon nanoposts with straight walls that enabled us to measure single platelet contractile forces. The arrays were replicated in PDMS (Fig. 9). Each nanopost in an array acts as a cantilever beam that bends in proportion to the force applied at its tip (Fig. 7).

To assess whether a platelet's cytoskeletal forces can be transmitted via the GPIb-IX-V complex, we measured the contractility of individual platelets using these arrays of flexible nanoposts described above. We coated the tips of the nanoposts with VWF and then

seeded human platelets onto the arrays. Platelets attached to the tips of the nanoposts, spread over multiple nanoposts, and deflected them via their cytoskeletal forces (Fig. 9a).

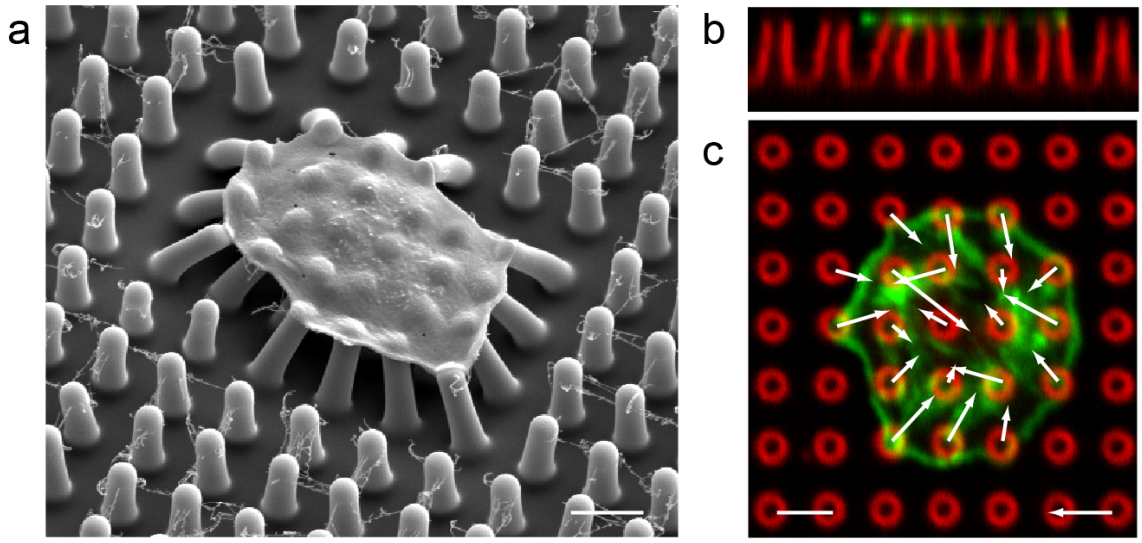

Figure 9 | Arrays of nanoposts to measure cytoskeletal forces in platelets. **a,** SEM image of a platelet on an array of nanoposts. **b,** Side-view and **c,** top-view from confocal microscopy of an individual platelet on nanoposts (green: actin, red: post). Scale bars are 2 μm and force scale bars are 3 nN.

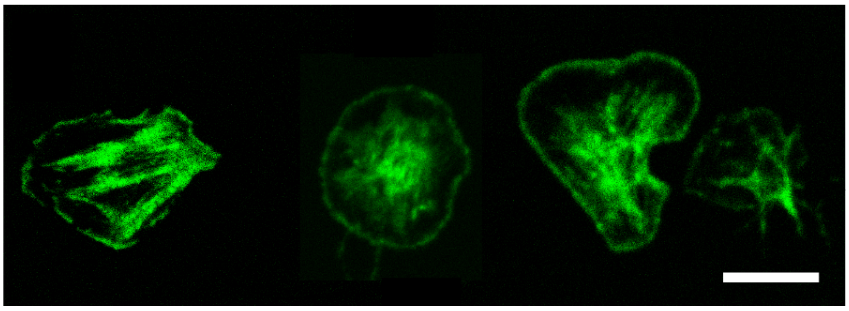

Figure 10 | Micrographs from confocal microscopy of platelets adhered onto flat surfaces of PDMS that were coated with VWF. Platelet morphologies on VWF as depicted by phalloidin staining are similar to that of platelets on nanoposts coated with VWF, as shown in Fig. 9c. Scale bar is 5 μm.

We measured the deflections of the nanoposts produced by platelets using confocal microscopy (Fig. 9b-c). The force on each nanopost was calculated according to Hooke's law. We noted that platelets on nanoposts had morphologies (Fig. 9c) that were similar to those of platelets on flat surfaces coated with VWF (Fig. 10), which indicated that the topology of the array did not impede the ability of the platelets to change shape or spread.

1.1.4 Discussion

Here, we report the development of a novel sensor, nanopost arrays, to measure single platelet forces. We demonstrate that nanopost arrays could be utilized to study the interaction of platelets with specific extracellular matrices such as VWF. Our control experiments confirm that the interaction of platelets with VWF-coated nanopost arrays is specifically through the binding of platelets to the VWF. The nanopost arrays provide a spatial resolution, which allows us to generates a force map for platelets and use that force map to calculate the contractile force of each platelet. Nanopost arrays are the first tool that enables the direct measurement of single platelet contractile forces on controlled matrices. Therefore, same techniques that were used in this work to study the interaction of platelets and VWF could be utilized to look at the interaction of platelets with other matrices such as fibrinogen (data not shown). This technology could be further used to measure platelet contractility in different donors as a gateway to personalized medicine. Nanopost arrays could also be used to isolate and investigate the effect of different agonist or antagonist treatments on platelet contractility. This can be combined with various antibody or small molecule inhibitor treatments to tackle different pathways that lead to platelet activation, adhesion, shape change, or contractility. As an alternative nanopost arrays could also be employed to pursue a deeper understanding in the mechanism of certain platelet-related disease and the role of platelet contractility in those disease e.g. VWF disease and Bernard Soulier syndrome.

Together, we believe that this technology has the potential to serve to answer a number of unanswered questions within the field of hemostasis and platelet biomechanics.

1.2 Determining the Role of Integrin $\alpha_{IIb}\beta_3$ and GPIb-IX-V in Transmitting Cytoskeletal Forces in Platelets

1.2.1 Background

VWF is a multi-domain protein that contains binding sites for both GPIb-IX-V complex (within its A1 domain) and integrin $\alpha_{IIb}\beta_3$ (within its C1 domain) [182]. According to previous studies, integrin $\alpha_{IIb}\beta_3$ transmits cytoskeletal forces within a clot and to the ECM by linking the cytoskeleton to its corresponding ligands through focal adhesion proteins such as talin and vinculin. However, the GPIbα subunit of GPIb-IX-V complex also links the actin cytoskeleton to the A1 domain of VWF by a filamin link [40]. Previous evidence suggests that GPIbα binds to the A1 domain in a force sensitive manner. Specifically, the lifetime of GPIbα-A1 domain increases as the bond is stretched when external shear forces are applied [43]. To isolate the interaction of the platelets with VWF to only one receptor, we took the approach of using blocking antibodies to block the other receptor. We pre-treated platelets with monoclonal antibodies: AK2 to block GPIbα subunit of GPIb-IX-V complex and 7E3 to block $\alpha_{IIb}\beta_3$. AK2 has been widely used to block GPIb-IX-V binding to VWF to conduct studies such as GPIb-IX-V mediated platelet aggregation; GPIb-IX-V associated platelet rolling on VWF, and VWF self-association on platelets GPIb-IX-V under hemodynamic shear. Antibody 7E3, commercially known as abciximab, has been administrated clinically in patients undergoing high-risk percutaneous transluminal coronary angioplasty or directional coronary atherectomy to block $\alpha_{IIb}\beta_3$ irreversibly. To control for any other mechanism that may be involved but not considered, we ran controls blocking both receptors at the same time.

In order to measure the contractile forces of platelets that received each of these treatments, we used the described VWF-coated nanopost arrays. We investigated the contractile forces of platelets that received each of these treatments to quantify the contribution of each of the two receptors in force transmission. We **hypothesized** that platelet contractile forces are transmitted to VWF through *both* GPIb-IX-V complex and $\alpha_{IIb}\beta_3$ receptor. Furthermore, we **hypothesized** that GPIb-IX-V transmits cytoskeletal forces by binding to VWF's A1 domain using its GPIbα subunit.

1.2.2 Methods

Antibody Treatment

Platelets were isolated as outlined in methods section 1.1.2. We incubated platelets in Tyrode's buffer with AK2 (5 μg/mL, Abcam, Cambridge, MA), 7E3 (20 μg/mL, courtesy of Barry Coller, Rockefeller Univ.), both antibodies, or untreated for 20 minutes with gentle rocking. Immediately after incubation with antibodies, platelets were seeded onto arrays of nanoposts submerged in Tyrode's buffer. To determine if treating the platelets with antibodies caused them to activate, we analyzed the samples of platelet with flow cytometry.

Nanopost Fabrication and Functionalization

Arrays of silicone microposts were fabricated as described in methods section 1.1.2. The arrays of PDMS nanoposts were made onto glass slides. VWF was deposited on the tips as described in methods section 1.1.2.

Constructing pBIG-4e and pBIG-4f

The cDNA encoding green fluorescent protein (GFP) was excised from plasmid pEGFP-N1 (Clontech Laboratories, Mountain View, CA; Genbank accession no. U55762) by digestion with SalI and NotI restriction endonucleases and ligated into the corresponding restriction sites of plasmid pIRES (Clontech Laboratories) to generate vector pBIG-St1. The IRES-GFP cassette was excised from pBIG-St1 by digestion with NotI, blunt-end fill-in with T4 DNA polymerase, and subsequent digestion with NheI. The resulting fragment was ligated into pBI (Clontech Laboratories; Genbank accession no. U89932), which had been digested with NheI and EcoRV. The resulting vector was designated pBIG-St2. The DNA sequence encompassing the Kozak sequence, start codon, and the coding sequence of the bovine prolactin signal peptide and BirA (E. coli biotin ligase) were amplified by PCR from plasmid pCBioSec 27 and ligated into plasmid pBIG-St2 that had been digested with PstI and NotI. The resulting vector was designated pBIG-St3. Finally, the Kozak sequence, start codon, α1-antitrypsin signal peptide coding sequence, multiple cloning site (MCS) and biotin acceptor peptide (BioTag) 28 coding sequence of plasmid pCBioSec were PCR amplified and ligated into plasmid pBIG-St3 that had been digested with NheI and NsiI. The resulting vector was designated pBIG-4e. Plasmid

pBIG-4f was constructed in a similar manner, except that a DNA sequence encoding an epitope tag for antibody HPC4 29 was inserted 5' to the BioTag sequence.

Recombinant GPIbα-300 G233V (Ibα300gof)

A partial cDNA encoding amino acids 1-300 of GPIbα that contain a gain-of-function G233V mutation 17 was PCR amplified and cloned into the NheI and XhoI sites of pBIG-4f. Correct insertion of GPIbα300-G233V was verified by sequencing, CHO Tet-On cells (Clontech, Mountain View, CA) were stably transfected with pBIG-4f-Ibα300gof and pUC19-puromycin to enable selection of stably expressing cell lines. Recombinant Ibα300gof was produced as follows. Cells expressing the mutant were incubated for 48 hours in serum-free medium (EX-CELL 302; Sigma, Bloomington, MN) containing 10 μM biotin (Sigma) and 2 μg/mL doxycycline (Sigma). The medium was the concentrated, and desalted to remove free biotin using a PD-10 column (Sigma). The VWF-coated nanoposts were incubated with Ibα300gof (170 μg/mL) for 20 minutes to block the A1 domain of VWF. Experiments with platelets seeded onto arrays of nanoposts pretreated with Ibα300gof were conducted in an identical manner to experiments with full-length VWF coatings as described above.

Recombinant A1 domain of VWF

A cDNA encoding amino acids 1260-1471 of VWF that comprise its A1 domain was PCR amplified and cloned into the PstI and XhoI sites of pBIG-4e. Correct insertion of A1 was verified by sequencing. CHO Tet-On cells (Clontech, Mountain View, CA) were stably transfected with pBIG-4e-A1 and pUC19-puromycin to enable stable selection. Recombinant A1 was produced by first incubating the cells in serum-free medium (EX-CELL 302; Sigma, Bloomington, MN) containing 10 μM biotin and 2 μg/mL doxycycline for 48 hours, then concentrating and desalting the medium using a PD-10 column to remove free biotin.

CHO Tet-on cells were grown to 30% confluence and incubated with serum-free medium containing 10 μg/mL biotin and 10 μM doxycycline for 48 hours at 37°C. The conditioned media was collected, concentrated and desalted. To determine protein concentration, serial dilution of the recombinant protein and biotinylated BSA standards were sepa-

rated by SDS-PAGE and detected using streptavidin-HRP. Densitometric analysis was used to determine protein concentration (Fig. 11).

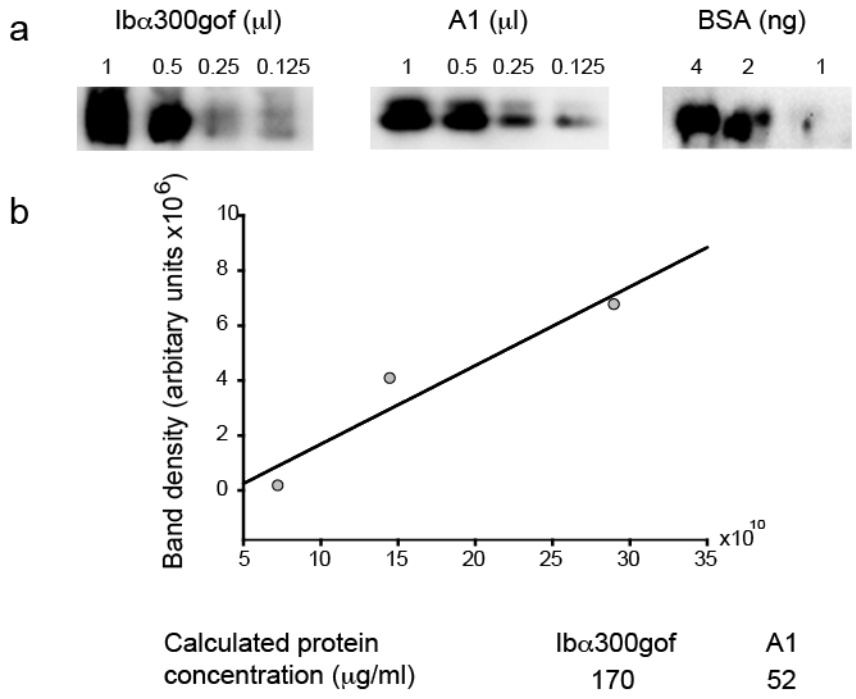

Figure 11 | a, Representative immunoblots of Ibα300gof, A1, and biotin-BSA. **b,** Calculated protein concentration using the standard curve for Ibα300gof and A1.

Functionalizing Nanoposts with Recombinant A1 domain

To capture the biotinylated recombinant A1 domain at the tips of the nanoposts, we stamped streptavidin (10 μg/mL; Calbiochem, Darmstadt, Germany) onto the tips of the nanoposts using microcontact printing. After treating the nanoposts with Alexa Fluor 594–conjugated BSA and 0.2% Pluronic F-127, nanoposts were submerged in a solution containing recombinant A1 domain (52 μg/mL) for 20 minutes. Experiments with platelets seeded onto arrays of nanoposts coated with recombinant A1 were conducted in an identical manner to experiments with full-length VWF coatings as described above.

Contractility Analysis

For these studies, confocal microscopy was used to obtain z-stacks of platelets on the nanopost arrays. The top and bottom images were extracted from the z-stacks. The forces were measured as described in methods section 1.1.2.

Statistical Analysis

R software was used for the statistical analysis. A linear regression model was used to assess the differences between platelet experiments. The model accounts for donor variability as a random factor. The level of significance was defined as a p-value less than 0.05. Error bars shown in figures are standard error of the mean calculated based on the number of replications.

1.2.3 Results

We observed that the forward and side scatter profile of untreated and antibody-treated platelets were similar, which indicates that the antibody pretreatment did not induce platelet activation (Fig. 12) and therefore, all the measurements were done on platelets that were contact activated as they were exposed to the VWF present at the tips of the nanoposts.

For each experimental cohort, we analyzed platelet morphology, spread area, and contractile forces (Table 1).

Forces on VWF were found to be higher in magnitude than values reported previously from single platelet studies measured on fibrinogen coatings [57]. For each donor, we normalized the data with respect to the results for untreated platelets to account for donor-to-donor variability in platelet function. Inhibition of GPIbα with AK2 did not affect platelet morphology (Fig. 13b), but it did significantly decrease the spread area of platelets (Fig. 13e).

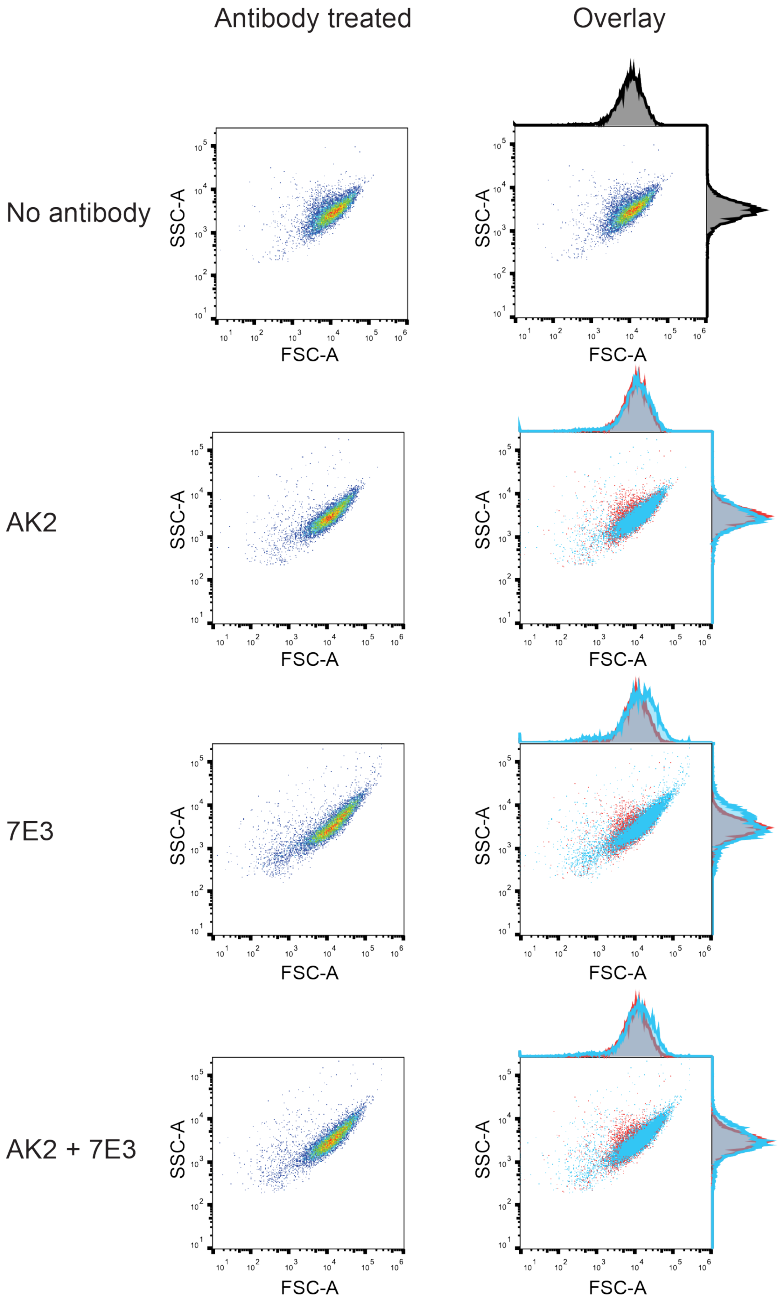

Figure 12 | To ensure that AK2 and 7E3 antibodies do not activate platelets, we assessed the samples of platelets before and after antibody incubation by flow cytometry. Dot plots and extracted histograms show that there is no change in the forward and side scatter of the platelets, indicating that the platelets were not activated by the treatment.

Table 1 | Measured Force and Spread Area per Donor for Antibody Study

	Force (nN)				Area (μm^2)			
Subject	*Control*	*AK2*	*7E3*	*AK2+7E3*	*Control*	*AK2*	*7E3*	*AK2+7E3*
Donor 1	53.2±40.2 (20)	45.8±37.4 (27)	19.7±23.5 (29)	4.6±1.7 (35)	28.0±16.4 (20)	21.4±13.3 (27)	12.3±8.5 (29)	5.4±1.4 (35)
Donor 2	100.3±33.3 (7)	80.7±35.0 (14)	46.3±28.5 (7)	*	40.8±18.2 (7)	25.8±12.4 (14)	27.6±13.7 (7)	*
Donor 3	26.1±18.5 (20)	25.4±16.8 (24)	16.7±20.1 (20)	13.5±13.1 (15)	24.3±14.9 (20)	25.0±15.4 (24)	14.4±12.1 (20)	15.6±11.6 (15)
Donor 4	33.3±26.5 (18)	26.9±29.0 (11)	26.2±32.4 (8)	8.5±10.8 (4)	28.8±21.2 (18)	21.1±17.9 (11)	17.3±16.2 (8)	13.0±8.5 (4)
Donor 5	76.0±41.3 (12)	46.1±39.7 (27)	12.5±18.2 (18)	16.4±25.8 (20)	38.0±19.0 (12)	21.0±19.4 (27)	8.0±5.5 (18)	8.8±9.4 (20)

Results per donor for these studies are shown as mean ± standard deviation. The number of platelets analyzed per condition are shown in parentheses. The normalized results are shown in Fig. 13. Asterisk (*) indicates that platelets did not adhere to the array.

We found that treating platelets with AK2 reduced the transmission of cytoskeletal forces by 19% (Fig. 13f). In contrast, inhibition of $\alpha_{IIb}\beta_3$ with 7E3 caused platelets to develop a dense actin core, numerous filopodia, and defective lamellipodia (Fig. 13c). This morphology was expected given that lamellipodial formation in platelets requires the engagement of $\alpha_{IIb}\beta_3$ with its ligand. Platelets treated with 7E3 displayed significantly reduced spread area (Fig. 13e) and cytoskeletal force transmission (Fig. 13f) as compared to untreated platelets or AK2-treated platelets. However, the contractile forces were not abolished completely with $\alpha_{IIb}\beta_3$-inhibition since platelets retained 48% of the force produced by untreated platelets. When platelets were treated with both AK2 and 7E3, very few platelets attached to the nanoposts, and those that did attach were rounded (Fig. 13d), poorly spread (Fig. 13e), and transmitted less force than untreated platelets, AK2-treated platelets, or 7E3-treated platelets (Fig. 13f). These results suggested that in addition to αIIbβ3, GPIb-IX-V supports a portion of the cytoskeletal forces transmitted to VWF.

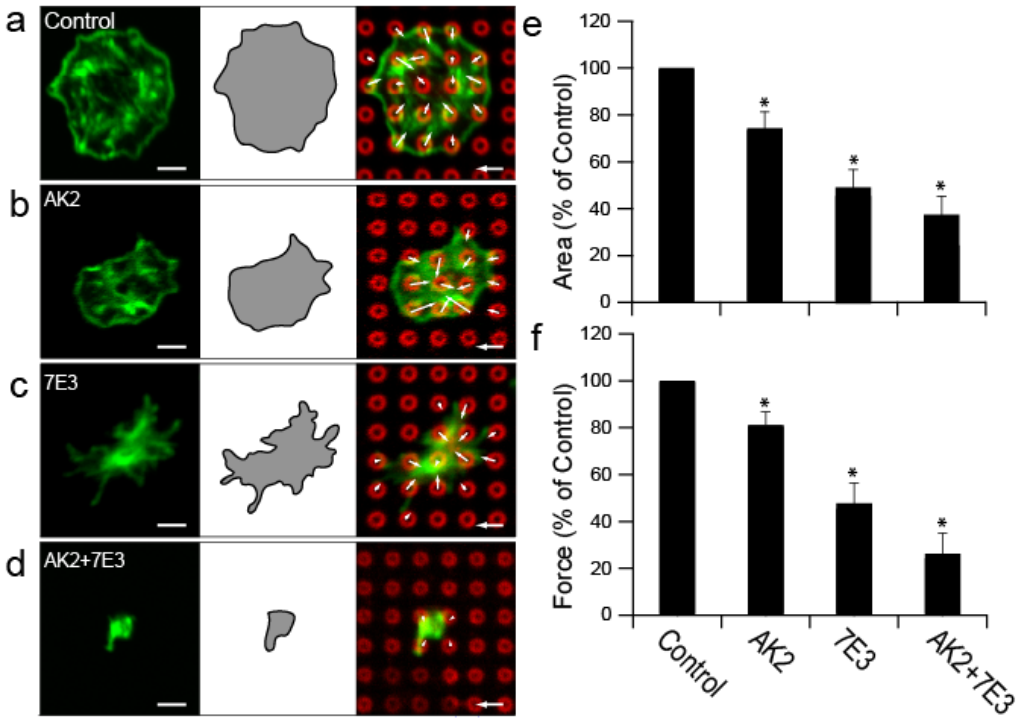

Figure 13 | Integrin $\alpha_{IIb}\beta_3$ and GPIb-IX-V can transmit cytoskeletal forces in platelets. **a**, no treatment (control), **b**, GPIbα-blocking antibody (AK2), **c**, $\alpha_{IIb}\beta_3$-blocking antibody (7E3) or **d**, both antibodies (AK2+7E3). **e**, Platelet spread areas and **f**, cytoskeletal force are shown relative to the control condition in each experiment (N = 5 replicates). Scale bars are 2 μm and force scale bars are 3 nN.

To occupy the A1 domain of VWF so that GPIb-IX-V binding is inhibited, we used an N-terminal GPIbα polypeptide (Ibα300gof) that contains a gain-of-function mutation (G233V) for spontaneous binding to VWF. Blocking the A1 domain of VWF with Ibα300gof did not affect platelet morphology (Fig. 14a-b), but it did reduce their spread area (Fig. 14d) and transmission of cytoskeletal forces (Fig. 14e).

As another approach to measure cytoskeletal forces associated with GPIb-IX-V, we immobilized recombinant A1 domain of VWF onto the tips of the nanoposts. Platelets that adhered onto recombinant A1 domain had morphologies that were similar to platelets on PDMS surfaces coated with recombinant A1 domain (Fig. 15).

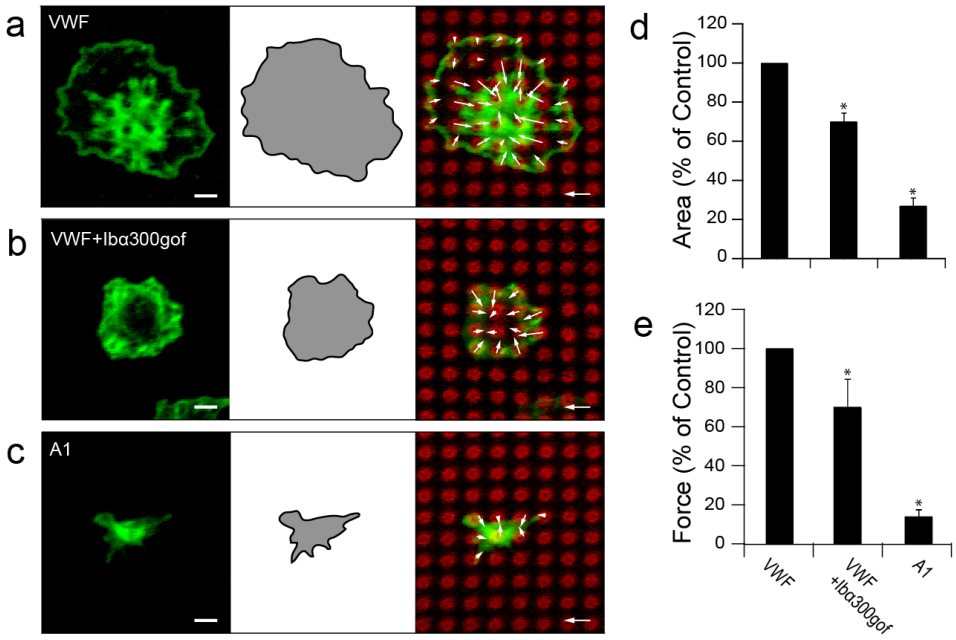

Figure 14 | GPIbα-A1 domain bond transmits platelet cytoskeletal forces. Representative image of a platelet on VWF-coated nanopost arrays coated with **a,** VWF (control), **b,** VWF treated with recombinant peptide for GPIbα (Ibα300gof), or **c,** recombinant A1 domain (green: actin, red: post). **d,** Platelet spread area and **e,** cytoskeletal forces are shown relative to the control condition in each experiment (N = 5 replicates). Scale bars are 2 μm and force scale bars are 3 nN.

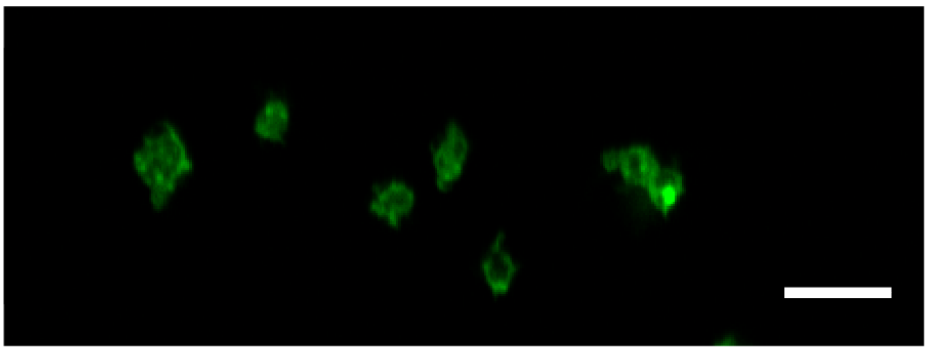

Figure 15 | Micrographs from confocal microscopy of platelets adhered onto flat surfaces of PDMS that were coated with recombinant A1 domain. Platelet morphologies on A1 domain as depicted by phalloidin staining are similar to that of platelets on nanoposts coated with A1 domains shown in Figure 13c. Scale bar is 5 μm.

We noted that the morphology of platelets on recombinant A1 resembled that of 7E3-treated platelets on VWF (Fig. 12c), which indicates that interactions between $\alpha_{IIb}\beta_3$ and VWF were sufficiently inhibited. Platelets that adhered onto recombinant A1 spread less than platelets that were VWF (Fig. 13a and Table 2).

Table 2 | Measured Force and Spread Area per Donor for Recombinant Protein

	Force (nN)			**Area (μm^2)**		
Subject	*Control*	*Iba300gof*	*A1*	*Control*	*Iba300gof*	*A1*
Donor 1	42.9±29.1 (33)	38.8±29.4 (24)	10.8±7.8 (29)	25.7±16.5 (33)	21.3±15.4 (24)	9.0±7.1 (29)
Donor 2	86.8±64.1 (19)	38.0±39.1 (30)	16.3±13.7 (36)	37.4±28.7 (19)	25.7±22.1 (30)	11.3±6.8 (36)
Donor 3	47.2±26.4 (32)	14.5±15.8 (33)	2.5±0.8 (36)	24.1±14.8 (32)	12.7±8.9 (33)	4.9±1.8 (36)
Donor 4	45.2±20.0 (22)	43.1±20.4 (24)	10.3±5.8 (25)	25.0±12.4 (22)	17.2±10.4 (24)	8.0±3.2 (25)
Donor 5	47.4±27.0 (24)	41.9±23.5 (30)	1.8±0.6 (18)	20.7±12.4 (24)	16.5±8.6 (30)	3.5±2.1 (18)

Results per donor for these studies are shown as mean ± standard deviation. The number of platelets analyzed per condition are shown in parentheses. The normalized results are shown in Fig. 14.

Platelets on recombinant A1 domain generated contractile forces that were 15% of those obtained on full-length VWF (Fig. 14e and Table 2).

1.2.4 Discussions

Numerous roles has been identified and described for GPIb-IX-V complex. However, the studies conducted here led to the discovery of a force transmission role for GPIb-IX-V complex that had never been described before. AK2 and 7E3 blocking antibodies provided a means to isolate the interaction of platelets with the multimeric VWF by blocking GPIb-IX-V and $\alpha_{IIb}\beta_3$, respectively. Blockage of each of these receptors led to partial re-

duction of force transmission, hinting for the contribution of both receptors in force transmission. Simultaneously blocking both receptors supported our original hypothesis that there is not a significant third player that is not examined in this study.

Recombinant Ibα300gof blocked the interaction of GPIb-IX-V complex on platelets with VWF by preoccupying the A1 domain sites on the VWF coating. These experiments mirrored the AK2-blocked platelet force measurements in which, the AK2 treatment inhibited the interaction of the GPIb-IX-V complex with the A1 domain by blocking the complex on the platelet membrane and Ibα300gof blocked the interaction by occupying the available A1 domains on the VWF coating. These studies confirmed our finding with the antibody studies.

The origin of force reduction in platelets still remains a mystery despite both the blocking antibody studies and Ibα300gof assays. In other words, whether the reduction in forces is due to the inhibition of known functions of GPIb-IX-V complex such as signaling for and eventually activating $\alpha_{IIb}\beta_3$ or whether it is inhibition of direct force transmission through the complex via its filamin link to the actin cytoskeleton. Using A1 domain as the coating on the nanoposts we clarified the particular contribution of GPIb-IX-V by isolating the interaction of platelets and VWF to the GPIbα-A1 domain and therefore, excluding any potential indirect role of GPIb-IX-V complex inhibition on platelet contractility or force transmission through $\alpha_{IIb}\beta_3$. Platelets generated significant amounts of forces on the A1 domain demonstrating that independent of its other roles, GPIb-IX-V complex is capable of transmitting cytoskeletal forces.

Here, we identified a direct role for GPIb-IX-V complex in transmitting platelet contractile forces. The question yet to be answered is the physiological meaning of this new role for GPIb-IX-V complex *in vivo*.

1.3 Examining the role of Cytoskeletal Force Transmission of GPIb-IX-V in Platelet Adhesion to VWF

1.3.1 Background

The GPIbα subunit of GPIb-IX-V complex has a catch bond behavior as it binds to VWF's A1 domain, i.e. the lifetime of the bond increases as the force is applied until the

bond transitions back to a slip-bond. Previously external hemodynamic forces were described to strengthen GPIbα-A1 domain bond, as platelets were anchored on the exposed VWF on the injured vessel wall [43]. These findings emphasized on the importance of applied forces in maintaining the bonds that form between A1 domain and GPIbα. This is consistent with the findings that identify a more substantial role for GPIb-IX-V complex in the formation and stability of hemostatic clots in smaller vessels at higher shear rates (smaller vessels).

Our findings show that in addition to being responsive to the application of force, GPIb-IX-V is capable of transmitting cytoskeletal forces. Therefore, we **hypothesized** that cytoskeletal forces support catch bonds *internally*. To test this hypothesis, we inhibited myosin activity by treating platelets with small molecule inhibitor, blebbistatin. We investigated the capability of platelets to maintain their adhesion to the A1 domain-coated surfaces in the absence of cytoskeletal forces.

1.3.2 Methods

Platelet Wash-off Experiments

Flat PDMS substrates were incubated with A1 domain for 2 hours. Substrates were then washed with PBS and blocked with 2% BSA in PBS for 1 hour, and then followed by incubation in 0.2% Pluronic F-127 in PBS for 1 hour at room temperature. Platelets were incubated with or without blebbistatin (10 μM) for 20 minutes and seeded onto either the A1-coated PDMS substrates or a PDMS substrate without A1 domain (as a control for non-specific adhesion). Unbound or loosely bound platelets were removed by washing the substrates in a segmented petri dish with PBS, 40 minutes after seeding. Samples were then fixed, permeabilized, and stained as previously described.

Visualization and Analysis

Platelet adhesion was visualized using a 60× oil immersion lens. Images were collected at 10 arbitrary locations on the substrate. The number of platelets per each 60× field of view was counted for each substrate.

1.3.3 Results

GPIbα-A1 domain catch bonds are known to play an important role in the attachment of platelets to sites of vascular injury. We examined whether GPIbα-A1 domain catch bonds serve another purpose: to allow cytoskeletal forces to strengthen platelet adhesion to VWF in the absence of externally applied force. Consistent with this possibility, we found that inhibition of myosin with blebbistatin significantly reduced platelet adhesion to surfaces coated with recombinant A1 in the absence of flow (Fig. 16 and Table 3), suggesting that internal forces from actin-myosin interactions enhance the bond between GPIbα and A1.

Thus, cytoskeletal forces generated inside platelets and transmitted through GPIb-IX-V can support the adhesion of platelets to VWF, particularly under conditions where external forces are absent.

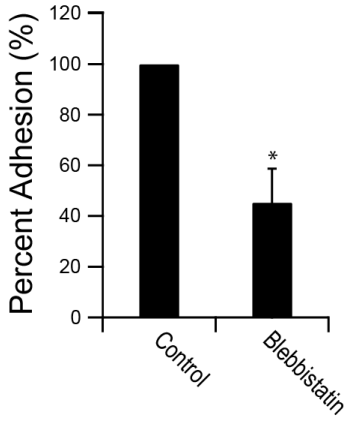

Figure 16 | Cytoskeletal forces are needed for platelet adhesion on A1 domain**.** Platelets adhered onto substrates coated with recombinant A1 domain had weaker adhesion strength when treated with blebbistatin as compared to untreated platelets (N = 4 replicates).

Table 3 |Platelet Count per Field

Subject	Control	Blebbistatin
Donor 1	12±5.7 (10)	7.8±8.5 (10)
Donor 2	8.7±8.5 (10)	1.3±0.8 (10)
Donor 3	4.9±9.1 (9)	1.5±2.8 (10)
Donor 4	1.9±1.1 (10)	1.3±0.9 (10)

The table shows platelet count per donor for adhesion assay shown in Fig. 16.

1.3.4 Discussions

The results from this study show that in the case where myosin is inhibited, platelets lose their capability to withstand a gentle wash, which represents the addition of an external force. The washing forces are similar to hemodynamic forces in physiologic conditions, which aim to detach platelets from the ligand-coated surface. Since the PDMS surface was coated with A1 domain and our control experiments show that platelet binding was only mediated through A1 domain-GPIbα interactions (Platelets did not bind to PDMS surfaces that were blocked and lacked A1 domain-coating), this can be further interpreted as platelets inability to maintain their A1 domain-GPIbα bonds in the absence of contractile forces. This finding suggests to a new physiological role for internal forces in catch bonds and in particular, for the A1 domain-GPIbα interaction.

AIM 2: EXAMINING THE MECHANISM OF GPIb-IX-V FORCE TRANSMISSION USING CHO CELLS

2.1 Examining the Role of GPIb-IX Complex in Transmitting Cytoskeletal Forces on A1 domain Compared to VWF

2.1.1 Background

Results from aim 1 indicate that GPIb-IX-V complex transmits cytoskeletal forces to VWF. In aim 2 we used CHO cells to investigate the mechanism by which GPIb-IX-V complex transmits cytoskeletal forces**.** CHO cells have been classically used to study the function and structure of GPIb-IX-V complex [183]. Wild type CHO cells do not express any receptor that binds to VWF. In order to model an isolated interaction between GPIb-IX-V complex and VWF in CHO cells, we used CHOαβIX cells, which are CHO cells that are transfected to stably express GPIbα, GPIbβ, and GPIX as previously described (Fig. 17) [183]. It has been previously shown that although these cells lack GPV, the GPIb-IX complex they express is fully competent to bind to VWF.

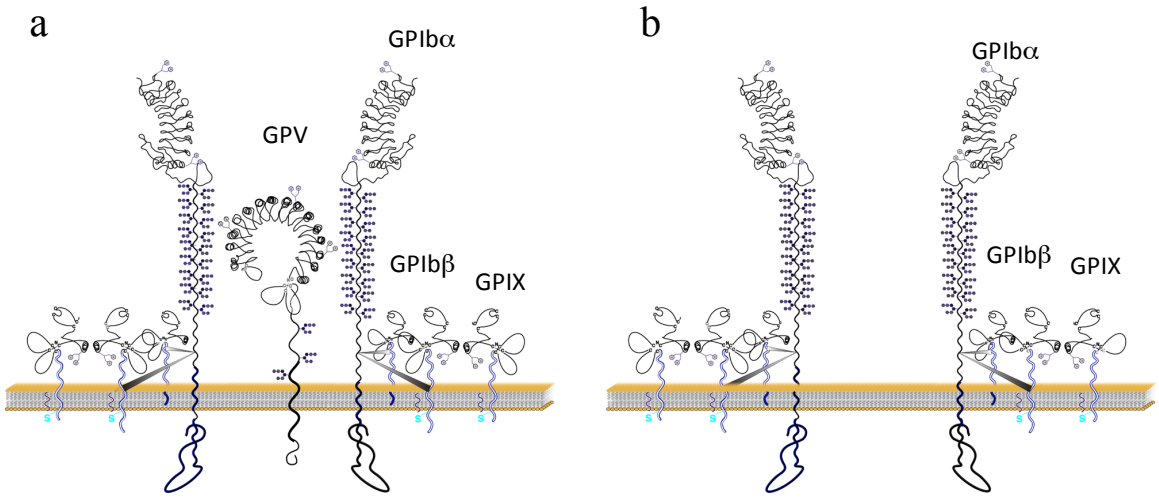

Figure 17 | a, GPIb-IX-V receptor expressed on platelet membrane, **b**, GPIb-IX receptor expressed on CHOαβIX cell membrane

Initially, we used CHOαβIX cells as a cellular model for platelets to determine whether GPIbα in another cellular context is capable of transmitting force to VWF similar to platelets. We further tested whether CHOαβIX cells could be used as a valid cellular model for this study. For this study we made micropost arrays, which are similar to nanopost arrays but are larger and more widely spaced to adjust for the bigger size of these cells compared to platelets. The tips of microposts were coated with either full length VWF or recombinant A1 domain. We **hypothesized** that CHOαβIX cells generate similar forces on both VWF and recombinant A1 domain coatings since the only VWF-binding receptor they express is GPIb-IX complex.

2.1.2 Methods

Fabrication of Micropost Array SU-8 Master

The process of fabricating arrays of microposts has been previously described {Sniadecki, 2007 #178}. In brief, a silicon wafer was spin-coated with a 5-μm layer of SU-8 2005 (MicroChem Corp., Newton, MA). The base layer of resist was flood-exposed with UV light to cross-link the SU-8. The wafer was spin-coated with a 7-μm layer of SU-8 2010. A chrome mask containing the features of the microposts was used to selectively expose the second layer of SU-8 with UV light. The unexposed regions in the SU-8 layer were removed using SU-8 developer (MicroChem Corp.) to make arrays of microposts that were 2.39 μm in diameter, 6 μm in spacing and 6.98 μm in height.

To make PDMS replicates of the microposts, we used a double casting process that was similar to the process for PDMS nanoposts. The arrays of PDMS microposts were baked for 6 hours at 110°C, yielding a Young's modulus of 3.1 MPa for PDMS. Therefore, the bending stiffness of micropost arrays was calculated to be 43.6 nN/μm for the first array.

Functionalizing Microposts with VWF

A microcontact printing technique was used to transfer VWF onto the tips of the microposts in a similar manner to what has been described before[181]. In brief, we baked a 1-cm layer of PDMS (30:1 ratio of base-to-curing agent) against a passivated silicon wafer for 10 minutes at 110°C and cut it to make stamps for transferring protein to the tips of the microposts. Stamps were coated with droplets of VWF (10 μg/mL in PBS) for 2

hours to allow for protein adsorption, washed in DI water, and then dried. To make the surface of the microposts hydrophilic and facilitate the transfer of protein, we treated the microposts with UV ozone (Jelight, Irvine, CA) for 7 minutes. The stamps were then placed in full contact with the tips of the microposts in order to transfer VWF onto them. We then treated the uncoated surfaces of the arrays with Alexa Fluor 594-conjugated BSA and 0.2% Pluronic F-127 in a similar manner as described for preparing arrays of nanoposts.

Coating Microposts with A1 domain

To capture the biotinylated recombinant A1 domain at the tips of the microposts, we stamped streptavidin (10 μg/mL) onto the tips of the microposts using microcontact printing in a similar manner to VWF. After the blocking steps with Alexa Fluor 594-conjugated BSA and 0.2% Pluronic F-127 were completed, we submerged the microposts in a solution containing recombinant A1 domain (52 μg/mL) for 20 minutes to allow for the biotin tag to bind the streptavidin on the microposts.

CHO Cell Line

The CHOαβIX cells were produced as described. Briefly, the wild type GPIbα construct was transfected into CHO cells stably expressing GPIbβ and GPIX (CHOβIX) along with pREP4 (Invitrogen, Carlsbad, CA), which carries a hygromycin-resistant marker. We used flow cytometry to assess the expression of GPIX and GPIbα subunits with anti-CD42a and anti-CD42b (BD Biosciences, Franklin Lakes, NJ), respectively (Fig. 18).

Mouse IgG (BD Biosciences) was used as a control. CHO cell line was maintained in DMEM (Sigma, Bloomington, MN), 10% FBS (Sigma), L-glutamine (2 mM; Sigma), 1% pen/strep (Sigma), G418 (400 μg/mL; Sigma), methotrexate (80 μM; Sigma), hygromycin (100 μg/mL; Sigma).

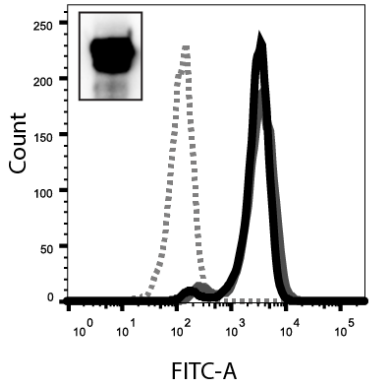

Figure 18 | Expression of GPIbα and GPIX subunits in CHO cells. CHOαβIX cells were incubated with anti-CD42a (GPIX), anti-CD42b (GPIbα) or mouse IgG. Surface expression of GPIbα in the cells was assessed by flow cytometry. Cell lysates were assessed for GPIbα protein by immunoblotting with the anti-GPIbα monoclonal antibody WM23. Flow cytometry histogram of cell surface expression of GPIbα and GPIX in CHOαβIX cells. Grey dotted line denotes IgG, solid grey line denotes GPIX, and solid black line denotes GPIbα. Insets show immunoblot for GPIbα.

CHO Cell Experiments

A volume of 300 µl CHOαβIX cells (5×10^5/mL in serum free media (EX-CELL 302; Sigma, Bloomington, MN) were diluted to 3 mL with serum free media to a concentration of 5×10^4/mL and incubated with the microposts for 16 hours at 37 °C in 5% CO_2 in the presence of ristocetin (1.5 mg/mL, abc Limited, NJ). We washed the cells on the micropost arrays with PBS, fixed, permeabilized them in PBS containing 4% paraformaldehyde and 0.1% Triton X-100 for 30 minutes, and stained the cells with FITC-phalloidin (1:200 in PBS) for 30 minutes.

Control Experiments

To check for the specificity of the binding of CHOαβIX cells to the micropost arrays coated with A1 domain or VWF, we designed several control experiments where we seeded the cells on microposts that were treated with the blockers and did not have either of the target proteins on them. CHOαβIX cells failed to adhere to micropost arrays that were blocked with Alexa Fluor 594-conjugated BSA and 0.2% Pluronic F-127. Further-

more, we used CHO cells that are stably expressing GPIbβ and GPIX (CHOβIX). These cells failed to adhere to microposts coated with A1 domain or VWF.

Force and Spread Area Analysis

A manual code was developed in MATLAB to analyze the images of the samples obtained from fluorescent microscopy similar to aim 1.

We calculated the total force per cell by summing the magnitudes of the force vectors at each micropost underneath the cell. We then divided that with the number of posts that were covered by the cell to normalize for the effect of treatment on the spreading of the cells and generated the force per post quantity.

Spread area was quantified from the actin image using the outer edge of the cell on the posts similar to aim 1.

Statistical Analysis

R software was used for the statistical analysis. A linear regression model was developed to assess the differences between experiments. The model accounts for date of the experiment as a random factor. The level of significance was defined as a p-value less than 0.05. Error bars shown in figures are standard error of the mean calculated based on the number of replications.

2.1.3 Results

CHOαβIX cells adhered and spread on microposts that were coated with either VWF (Fig. 19a) or recombinant A1 domain (Fig. 19b).

CHOαβIX cells did not spread to the same degree on the two coatings (Fig. 18c), but generated contractile forces of similar magnitude (Fig. 18d). The similarity in the forces that they generated on the two coatings indicated that the GPIbα transmits forces to VWF. To confirm that the CHOαβIX cell forces measured on VWF and A1 domain are specifically transmitted through the GPIbα-A1 domain interaction, we used CHOβIX cells together with CHOαβIX cells. CHOβIX cells did not adhere to the microposts (Fig. 19c-d).

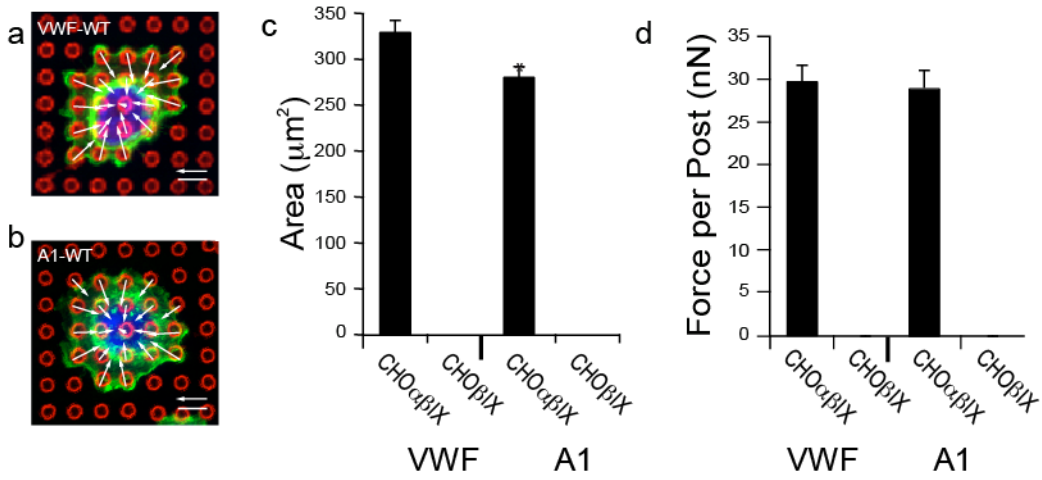

Figure 19 | CHO cells confirm the role of GPIbα in force transmission. Representative images of CHOαβIX cells on microposts coated with **a,** VWF, **b**, A1 domain. **c,** Spread area and **d,** cytoskeletal forces for CHOαβIX and CHOβIX cells (N = 5 replicates). Scale bars are 6 μm and force scale bars are 30 nN.

2.1.4 Discussions

CHOαβIX cells proved to be a valid cellular model for platelets in these experiments. They successfully bind VWF and A1 domain, spread and generate force. The failure of CHOβIX cells to adhere to either coating confirmed that GPIbα is the essential GPIb-IX-V subunit both accommodating adhesion and force transmission as they bind to VWF. Furthermore, the hypothesis was confirmed as CHOαβIX cells generated similar forces on the recombinant A1 domain and the VWF coatings. This finding demonstrates that the forces transmitted to the VWF via the GPIb-IX complex are specifically through the binding of this complex to the A1 domain of VWF. This observation could be considered a confirmation of the interpretations made in platelets (aim 1) in a different cellular context. Since the only VWF-binding mechanism in CHOαβIX cells is through GPIb-IX complex, other roles of this receptor in platelets (such as signaling and activating other platelet receptors) in mediating the forces that platelets generate on VWF coating is not a concern any more.

Here, CHOαβIX cells are identified as a suitable cellular model for GPIb-IX-V/VWF interaction; therefore we used them to study the mechanism by which GPIb-IX-V transmits contractile forces to VWF.

2.2 Examining The Role of Filamin A and Myosin In The Forces that Are Transmitted through GPIb-IX-V

2.2.1 Background

Cells generate mechanical forces by polymerization and de-polymerization of their structural proteins: actin and tubulin. Motor proteins such as myosins, kinesins and dyneins also generate mechanical forces by walking along actin and tubulin [19]. Platelets have a large pool of actin and myosin, and the GPIb-IX-V complex is in charge of 85% of the linkage between the membrane and actin cytoskeleton via a filamin A link [40]. In a separate study, we found that forces that are transmitted through the integrin $\alpha_{IIb}\beta_3$ are myosin-dependent. Previously, we found that GPIb-IX-V complex transmits cytoskeletal forces (Section 2.1). However, the nature of these forces and the role of filamin A are yet to be determined.

Here, we **hypothesized** that the forces transmitted through GPIb-IX-V complex to VWF are *myosin-dependent* forces and filamin A linkage plays a significant role in this force transmission. To test this hypothesis, we inhibited myosin activity in CHOαβIX cells and quantified the effect of myosin inhibition on their contractile forces. We further investigated the role of filamin A binding in transmitting these forces using CHOαΔ534βIX cell line (Fig. 20). CHOαΔ534βIX cells express the GPIb-IX complex but the complex has a truncation at the 534th amino acid of the GPIbα cytoplasmic tail which removes the binding site of the filamin A.

CHOαΔ534βIX cells are missing a portion of the cytoplasmic tail of the GPIbα subunit, which may be altering the behavior of the complex in more than one way and therefore reduce force transmission through mechanisms that are currently not known. To address this concern, we used CHOαFW-AAβIX cells, which contain a F568A and a W570A mutation. These residues are the hydrophobic residues that support the interaction between

GPIbα and filamin A. CHOαFW-AAβIX cells stably express the mutated complex but the GPIbα–filamin A interaction is completely disrupted in them [184].

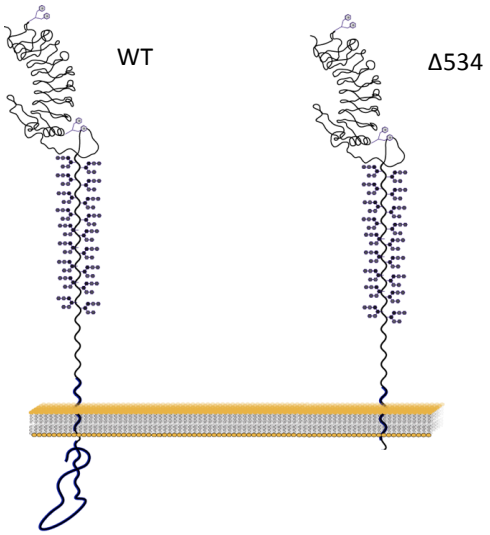

Figure 20 | GPIbα subunit in a, CHOαβIX cells, b, CHOαΔ534βIX cells

2.2.2 Methods

Fabrication of Micropost Array SU-8 Master

The SU-8 micropost arrays used for these experiments were developed as described previously. Microposts dimensions were 1.75 µm in diameter, 6 µm in spacing and 4.14 µm in height and yielded a stiffness of 54.9 nN/µm in PDMS replicates.

CHO Cell Lines

CHO cell lines were produced by Dr. Adam Munday at BloodWorks (former Puget Sound Blood Center). The CHOαΔ534βIX cells were produced as described. Briefly, the mutant GPIbα constructs were transfected into CHO cells stably expressing GPIbβ and GPIX (CHOβIX) along with pREP4 (Invitrogen, Carlsbad, CA), which carries a hygromycin-resistant marker.

In order to produce CHOαFW-AAβIX cells, mutation of F568 and W570 to A was achieved by using short overlap extension (SOE) PCR mutagenesis (Hoa SN, Hunt HD, Horton RM, Pullen JK and Pease LR. Site-directed mutagenesis by overlap extension using the polymerase chain reaction. 1989 77; 51-59) strategy, using the following mutagenic primer pairs: 5'-CTATAGGCTAGCATGCCTCTCCTC-3'and 5' GGCCGTAC-

CGCCAGGGCGAGGCTGG-3' and 5'-CCAGCCTCGCCCTGGCGGTACGGCC-3' and 5'-ACGCGTGAATTCTCAGAGGCTGTGGCCAGA-3'. F460-GPIbα (Shen Y, Cranmer SL, Aprico, A, Whisstock JC, Jackson, SP, Berndt, MC, and Andrews RK. 2006 JBC 281; 26419-26423) was used as a template for the PCR reaction. The two PCR products were gel purified and used as temple for the second PCR reaction using the external primers 5'-CTATAGGCTAGCATGCCTCTCCTC-3'and 5'-ACGCGTGAATTCTCAGAGGCTGTGGCCAGA-3'. The resultant PCR product was ligated into TOPT-TA (Life Sciences). Sequencing verified the correct mutation. the GPIbα cDNA was excised from TOPO-TA by digestion with NheI and EcoRI and ligated into the corresponding restriction sites of plasmid F460.

CHO cells expressing GPIbβ and GPIX (CHOβIX) were transfected with F460-GPIbα FW-AA using Fugene 9 (Roche, USA) according to the manufacture's directions. Cells were grown in the presence of puromycin (10 μg/ml) to establish stably expressing cells. We used flow cytometry to assess the expression of GPIX and GPIbα subunits after incubating cells with anti-CD42a and anti-CD42b (BD Biosciences, Franklin Lakes, NJ), respectively (Fig. 21).

Mouse IgG (BD Biosciences) was used as a control. CHO cell lines were maintained in DMEM (Sigma, Bloomington, MN), 10% FBS (Sigma), L-glutamine (2 mM; Sigma), 1% pen/strep (Sigma), G418 (400 μg/mL; Sigma), methotrexate (80 μM; Sigma), hygromycin (100 μg/mL; Sigma).

These experiments were conducted similar to section 2.1.2. We used micropost arrays that were coated with VWF in these experiments since previous results showed no difference in the forces of CHOαβIX cells on microposts coated with either recombinant A1 domain or VWF.

Cells treated with blebbistatin were incubated with blebbistatin (10 μM; Sigma) on the micropost arrays overnight at 37 ◦C.

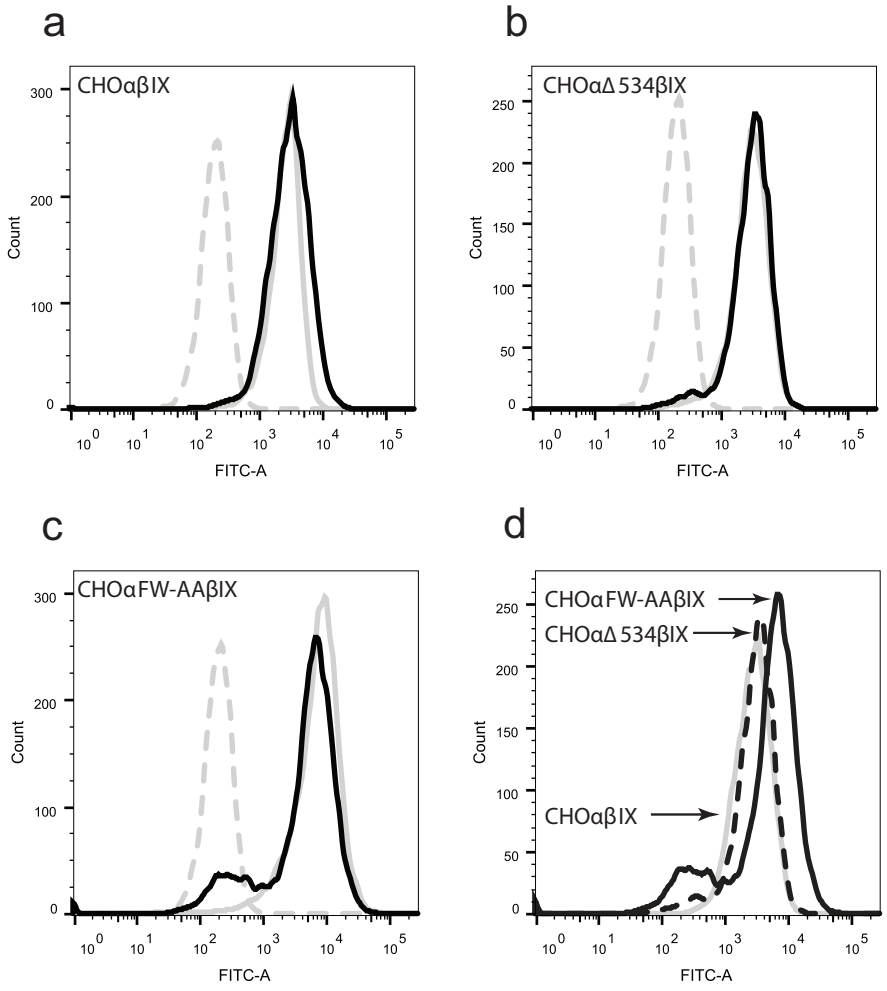

Figure 21 | Expression of GPIbα and GPIX subunits in CHO cells. CHOαβIX and CHOαΔ534βIX cells were incubated with anti-CD42a (GPIX), anti-CD42b (GPIbα) or mouse IgG. Surface expression of GPIbα in the cells was assessed by flow cytometry. Cell lysates were assessed for GPIbα protein by immunoblotting with the anti-GPIbα monoclonal antibody WM23. Flow cytometry histogram of cell surface expression of GPIbα and GPIX in **a,** CHOαβIX cells, and **b,** CHOαΔ534βIX cells **c,** CHOαFW-AAβIX cells. Grey dotted line denotes IgG, solid grey line denotes GPIX, and solid black line denotes GPIbα. **d,** Overlay of flow cytometry histograms of GPIbα surface expression from CHOαβIX (gray line) and CHOαΔ534βIX (dashed line) and CHOαΔ534βIX (black line) show that surface expression is similar in CHOαΔ534βIX and CHOαβIX cell lines and slightly higher in CHOαFW-AAβIX cell line.

2.2.3 Results

In order to test whether the contractile forces produced by CHOαβIX cells were generated by myosin motor activity, we treated the CHOαβIX cells with blebbistatin, an inhibitor of myosin's ATPase activity. CHOαβIX cells that received blebbistatin treatment spread more than the control (untreated cells) (Fig. 22a). Blebbistatin treatment significantly lowered the forces they produced on VWF-coated microposts (Fig. 22b). Together, these results indicate that cytoskeletal forces imparted onto the A1 domain of VWF act through the GPIbα subunit.

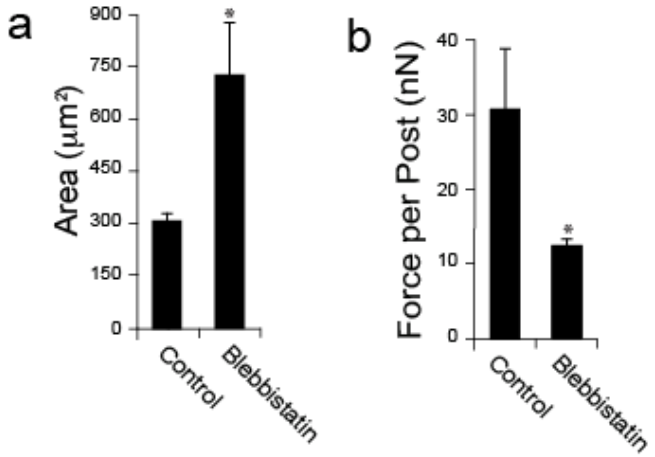

Figure 22 | GPIb-IX-V transmitted forces are myosin-dependent. **a,** Spread area and **b,** cytoskeletal forces of CHOαβIX cells treated with or without blebbistatin (N = 3 replicates).

We tested whether the actin–binding protein, filamin A, serves as an intermediary in transmitting cytoskeletal forces through GPIb-IX-V to VWF using CHO cells expressing a truncated version of GPIbα (CHOαΔ534βIX), which lack the binding site for filamin A. CHOαΔ534βIX cells adhered onto the microposts coated with VWF (Fig. 23a-b), but spread poorly (Fig. 23c). They exerted contractile forces that were significantly lower than the forces produced by CHOαβIX cells (Fig. 23d), implicating a role for filamin A in force transmission via GPIbα.

Truncation of cytoplasmic tail containing the filamin A binding site significantly reduced the forces in GPIb-IX transmitted contractile forces.

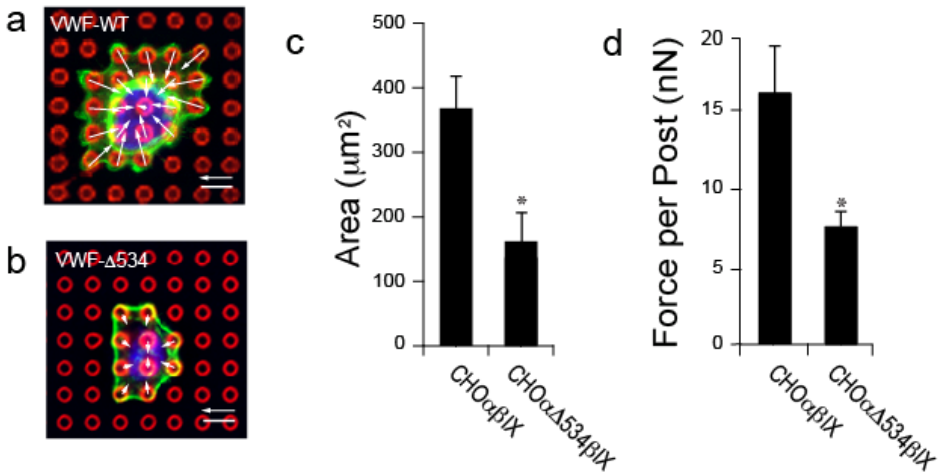

Figure 23 | CHOαΔ534βIX cells have reduced contractile forces on VWF. Representative images of **a**, CHOαβIX, **b**, CHOαΔ534βIX cells on microposts coated with VWF **c,** Spread area and **d,** cytoskeletal forces for CHOαβIX and CHOαΔ534βIX cells (N = 3 replicates). Scale bars are 6 μm and force scale bars are 30 nN.

To further study the particular role of filamin A, we used CHOαFW-AAβIX cells containing a F568A and a W570A mutation, which together inhibits the specific interaction of GPIbα and filamin A. CHOαFW-AAβIX cells adhered onto the microposts coated with VWF, and spread to higher degrees compared to CHOαβIX cells (Fig. 24a). They exerted contractile forces that were significantly lower than the forces produced by CHOαβIX cells (Fig. 24b).

CHOαFW-AAβIX cells generated similar forces to CHOαΔ534βIX cells on microposts coated with VWF. The similarity in their forces confirmed that the reduction in forces observed in CHOαΔ534βIX cells was specifically due to their inability to bind to filamin A and therefore the loss of the linkage of the complex to the actin cytoskeleton.

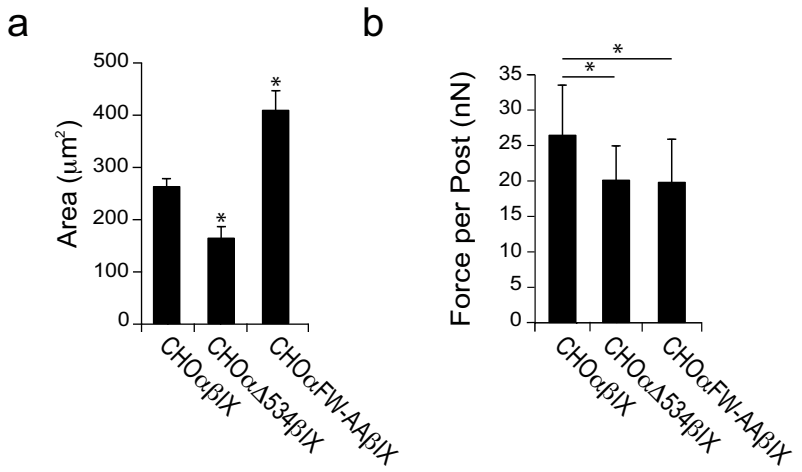

Figure 24 | Filamin A linkage plays a critical role in GPIb-IX-V transmitted forces. **a,** Spread area and **b,** cytoskeletal forces for CHOαβIX, CHOαΔ534βIX and CHOαFW-AAβIX cells (N = 5 replicates).

2.2.4 Discussions

Blebbistatin treatment prevents the ATPase activity of myosin. Therefore, the loss of contractility in blebbistatin-treated CHOαβIX cells on VWF-coated microposts indicates that these forces are myosin dependent. Together with our previous finding that these forces are transmitted through the GPIb-IX-V complex, it can be concluded that the forces transmitted through GPIb-IX-V complex are myosin-dependent.

Blebbistatin treatment also resulted in significantly higher spreading abilities of CHOαβIX cells on VWF-coated microposts. The reason for this effect is not fully understood, however, it is consistent with previous studies showing that myosin malfunction leads to extra large platelet production and higher spread areas in MYH9 platelets [185, 186].

Experiments conducted with CHOαΔ534βIX and CHOαFW-AAβIX cells targeted the specific role of the filamin A linkage of the GPIb-IX-V complex to the cytoskeleton. The partial truncation of the cytoplasmic tail of GPIbα in CHOαΔ534βIX cells significantly reduced the forces that were measured on VWF-coated microposts. Similarly double mutated CHOαFW-AAβIX cells resulted in identical reduction. Together these results can be interpreted as the role of filamin A in mediating force transmission through the GPIb-

IX-V complex. The mystery that remains unanswered in these studies is the mechanism by which the rest of the forces are supported in the absence of filamin A binding.

AIM 3 DETERMINING THE ROLE OF INTEGRIN $\alpha_{IIb}\beta_3$ AND GPIb-IX-V COMPLEX IN TRANSMITTING CYTOSKELETAL FORCES IN HEMOSTATIC CLOTS

3.1 Background

Hemostasis is initiated as individual platelets adhere to the exposed VWF at the wound site. As platelets bind, they get activated, release agonists such as ADP, causing the recruitment of more platelets to the platelet-rich clot that forms rapidly on the exposed subendothelium [187]. In this process, platelets use plasma soluble proteins such as fibrinogen and VWF to bind to other platelets via their integrin receptors as well as non-integrin receptors such as GPIb-IX-V complex [188]. The process of formation of the initial platelet-rich clot is often referred to as primary hemostasis. Once the primary hemostatic clot forms, secondary hemostasis begins with the rapid production of thrombin and consequently fibrin fiber mesh, which further strengthens the initial clot.

During primary hemostasis, two of the important adhesion receptors that govern the dynamics of platelet aggregation are GPIb-IX-V complex and integrin $\alpha_{IIb}\beta_3$. GPIb-IX-V is considered to be in charge of the initial transient binding of platelets to VWF, and their consequent rolling which is often followed by the engagement of $\alpha_{IIb}\beta_3$ and firm adhesion of platelets to form a stable aggregate. These receptors are also involved in platelet-platelet interactions within the aggregate as they bind to soluble fibrinogen and VWF.

Hemodynamic shear has been recognized as a factor that influences the dynamics of clot formation [6]. The current understanding is that GPIb-IX-V complex governs clot formation at higher shear rates compared to $\alpha_{IIb}\beta_3$, which is thought to be more important at low shear rates. Therefore, integrin $\alpha_{IIb}\beta_3$ is the primary receptor at low shear ($<2000\ s^{-1}$), while GPIb-IX-V becomes more dominant at higher shear ($>2000\ s^{-1}$).

The study of GPIb-IX-V in platelets (aim 1) and in CHO cells (aim 2) revealed a new role for this complex as it binds to VWF at the wound surface. However, the contribution of this receptor to the overall contractility of a clot is yet to be determined. In this aim we designed a microfluidic device to measure the contractile forces of micro-clots and used AK2 and 7E3 to block GPIb-IX-V and $\alpha_{IIb}\beta_3$, respectively. We **hypothesized** that similar

to single platelets, GPIb-IX-V complex partially supports the overall contractility of platelet aggregates.

3.2 Methods

Blood Collection

Fresh whole blood was collected in lithium heparin collection tubes (158 USP, BD Medical) from consenting donors under compliance with University of Washington donor regulations. Heparin was used over other anticoagulants such as ACD because it does not diminish the effective calcium within platelets [189]. Collected blood samples were kept in an insulating container on an orbital rocker to prevent cell separation in the blood as well as to equally distribute heparin within the tubes. Blood was used within 1 hour of collection.

Soft Lithography

The microfluidic device was fabricated in PDMS from an SU-8 master using soft lithography (Fig. 25a). The microchannels in the device were 1 cm long, 500 μm wide, and 55 μm tall. The blocks were situated along a 2-mm region at the midspan of each microchannel and each block is 10 μm long, 20 μm wide, and 15 μm tall. The microposts were located behind each of the blocks and are 4 μm in diameter and 15 μm in height (Fig. 25b-c). The array contained 96 pairs of blocks and microposts arranged in a staggered configuration in order to minimize the disturbance in the flow for the other blocks and posts downstream.

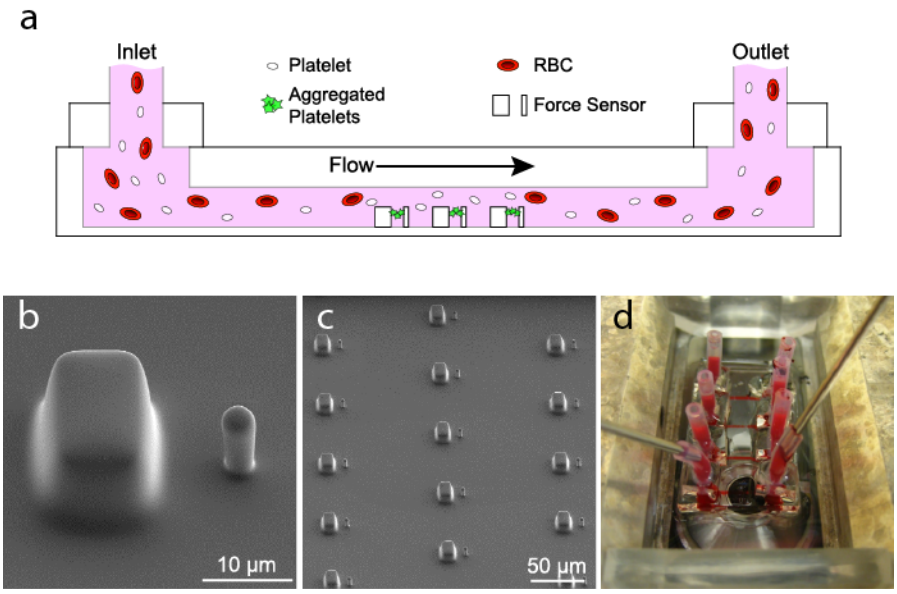

Figure 25 | Platelet forces measured on a microfluidic device. **a**, Schematic of microfluidic device to measure platelet contraction under shear. Whole blood is injected at the inlet and platelets adhere and aggregate to arrays of microscale blocks and posts. SEM micrograph of **b**, a block and post and **c**, an array of blocks and posts at the bottom of the microchannel. **d**, A macroscopic view of a device tested with whole blood on an inverted microscope.

Coating the Microchannel with VWF

The surface of the blocks, microposts, and walls of the microchannel were coated with Type I rat-tail collagen and purified human VWF to support platelet adhesion and activation. After coating the proteins, the blocks and microposts were treated with Δ9-DiI, which absorbed into the PDMS and allowed for the deflection of the microposts using fluorescence microscopy on an inverted microscope (Fig. 25d).

The shear rate in the microchannel was controlled by regulating the flow rate of blood as it was pumped using a syringe pump. The highest shear rates *in vivo* generally occur in small vessels, which have diameters from 10 to 50 μm and shear rates of 500 to 5000 s^{-1} [190, 191]. However, with larger diameter vessels, the effect of stenosis and occlusions can increase the shear rate to pathological levels of up to 50,000 s^{-1}[192, 193]. In another part of this study we studied the role of shear rate on the forces of clots that form between blocks and posts and found that the shear rate does not change the forces per area of the

aggregate but rather changes the rate of aggregation (Data not shown). The results indicated that force per area does not significantly change as we increase the shear rates from 2000 s^{-1} to 12000 s^{-1}. Therefore, we chose 8000 s^{-1} as the shear rate with which all the experiments were conducted. This shear rate mimics a low pathological shear rate.

Experimental Protocol.

Prior to testing, silicone tubing was used to connect the microfluidic device to a syringe on a syringe pump (New Era Pump Systems, Farmingdale, NY). The tubing and microfluidic device were pre-incubated with Tyrode's buffer for 1 hour prior to the start of an experiment. Blood was drawn from a collection container into a disposable syringe (BD Scientific, Franklin Lakes, NJ) through a wide opening to prevent shear activation and then loaded onto a syringe pump.

Antibody Treatment.

We incubated blood with AK2 (5 µg/mL, Abcam, Cambridge, MA), 7E3 (20 µg/mL, abciximab, ReoPro®;Eli Lilly, IN), both antibodies, or none for 20 minutes in small tubes with gentle rocking. Immediately after incubation with antibodies, blood was perfused in the microfluidic device.

Microscopy

The microfluidic devices were tested on a Nikon Eclipse Ti inverted microscope with 60× oil immersion objective enclosed in a Nikon live cell chamber maintained at 37 °C. Fluorescence and phase microscopy imaging was done with a cooled CCD camera (Andor Clara) with a Nikon TI-100 white light source and Nikon Intensilight C-HGFIE mercury lamp. During image capture, a phase image was taken every 20 seconds for recording the aggregate size, while fluorescence image at 594 nm was captured every second for tracking the deflection of the microposts.

Electron Microscopy

Samples for electron microscopy were prepared by flowing blood into the microchannel for 40 or 70 seconds. Afterwards, samples were fixed by incubating the samples in 3.5% paraformaldehyde in PBS. Critical point drying and microscopy steps were done similar to aim 1.

Force and Area Analysis

Micropost tracking was performed using a custom written MATLAB analysis program that compares the relative distance between the centroid positions of the fluorescently marked block and the micropost. There was no observable drag effect on the micropost from blood, even at high fluid velocities that corresponded with a shear rate of 12,000 s^{-1}. Using confocal microscopy, we confirmed that the block does not bend as the clot contracts. Platelet area was measured using Nikon NIS-Elements analysis tools to quantify the projected area of platelet aggregates downstream of the block structure. We concluded from these images that a dense packing of platelets would exert forces along the full length of the micropost, so the deflection of the micropost could be analyzed by assuming distributed load acting along the length of a fixed cantilever beam (Fig. 26)

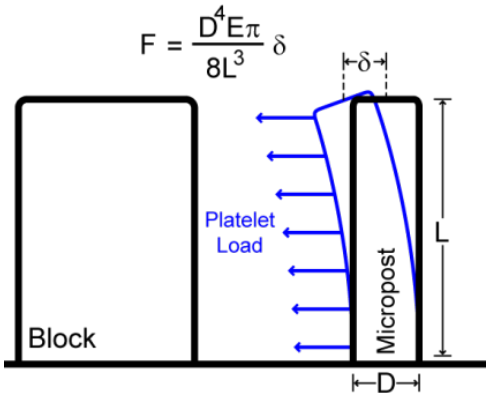

Figure 26 | Schematic of the deflection of the micropost due to platelet forces.

Statistical Analysis

Student's t-test was used for comparison between an experimental group and a control group, while ANOVA with a post-hoc test was used to compare the results for different shear rates. Data curves for force versus time or area versus time are shown as an average of at least 4 measurements per experiment and at least 3 replicate experiments. The dashed lines in the curve indicate the standard error of the mean.

3.3 Results

Microfluidic device to measure platelet forces under shear

To study platelet contractility during the formation of a hemostatic clot, a microfluidic device was developed to expose whole blood to hemodynamic shear in order to induce platelet aggregation between the arrays of microscale rectangular blocks and microposts in the microchannel (Fig. 27).

As blood entered the channel, platelets adhered to the blocks in the microchannel and formed hemostatic aggregates between blocks and microposts. We noted that individual platelets attached to the corners of blocks and directly behind the micropost first. After a few seconds, small strands of aggregated platelets formed that trailed behind the block or micropost in the flow stream. As the strands of platelets at the block grew in length and thickness, they filled the space between the block and micropost and formed a dense aggregate. Additional platelets attached to the outside of the aggregate over time, while platelets within the core of the aggregate were observed to visually transition towards the center of the clot. As the core shrunk, it bent the tip of the micropost towards the block.

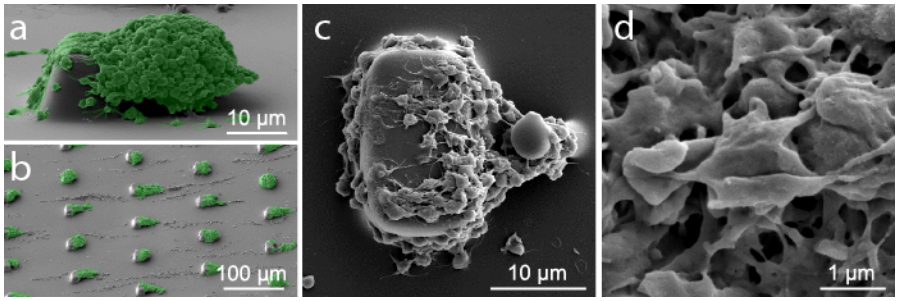

Figure 27 | SEM image of platelet aggregates **a**, on a block and post and **b**, on an array of blocks and posts after 70 seconds of blood flow. SEM image with **c**, a top-view and **d**, close-up view of a sensor with aggregated platelets after 40 seconds of blood flow.

The structure of the hemostatic aggregates formed in the microchannels after 70 seconds of flow were analyzed under SEM (Fig. 27a-b). They covered the gap between the blocks and microposts and had discoid platelets attached on their outer surface. Individual plate-

lets were also attached to the upstream side of the block and formed strands along the bottom of the microchannel. The clots that formed after 40 seconds of blood flow were smaller in size and did not have discoid platelets. The aggregated platelets had membrane tethers that extended to neighboring platelets in the clot and onto the block and micropost (Fig. 27c-d). Red or white blood cells were not found within the clots or attached to the blocks and microposts.

GPIb-IX-V complex and $\alpha_{IIb}\beta_3$ mediate force transmission in hemostatic clots.

To identify the contribution of GPIb-IX-V and $\alpha_{IIb}\beta_3$ in clot contraction, we pre-treated blood with AK2, or 7E3 (abciximab, ReoPro®) to block GPIb-IX-V complex or $\alpha_{IIb}\beta_3$, respectively. The blood was perfused in the microchannels at 8000 s^{-1} for 2 minutes.

AK2-treated blood formed smaller clots between the blocks and microposts. These clots were also less contractile compared to control (untreated blood) (Fig. 28a-b). Similar to AK2, 7E3 treatment also resulted in smaller clots that were less contractile than the control (Fig. 28c-d). Blood samples treated with both antibodies simultaneously, were mostly unable to form clots between blocks and micropost. The clots that were formed were not contractile (Fig. 28e-f).

Taken together, these results suggest that GPIb-IX-V is needed for a clot to form at high shear rates and these receptors play a role in platelet contraction. Additionally, these results confirm that $\alpha_{IIb}\beta_3$ is needed for the transmission of cytoskeletal forces in platelets during hemostasis.

3.3 Discussions

The tool developed here provides a unique way of directly measuring forces within hemostatic micro-clots. These results suggest a role for GPIb-IX-V receptor supporting clot contraction in addition to the known $\alpha_{IIb}\beta_3$-mediated mechanism. The diminishment of contractile forces in the presence of AK2 suggests that these clots are mostly VWF-mediated. However questions remain on the reason for which inhibiting each of the receptors lead to diminishment of the forces. This may hint to a synergic effect between the GPIb-IX-V complex and $\alpha_{IIb}\beta_3$ in terms of clot contraction that requires further studies.

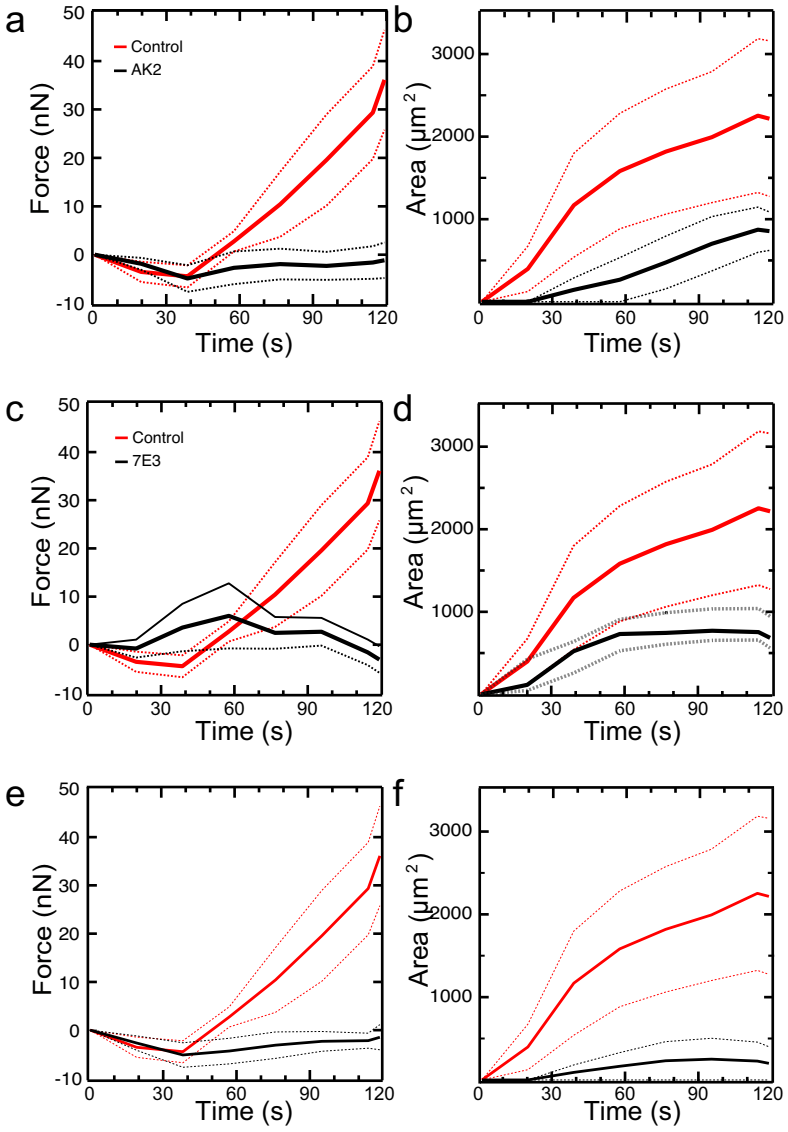

Figure 28 | Receptors GPIb-IX-V and $\alpha_{IIb}\beta_3$ have a role in platelet aggregate forces and size. Whole blood was incubated with **a-b**, AK2 to block GPIb-IX-V, **c-d**, 7E3 to block $\alpha_{IIb}\beta_3$, or **e-f**, 7E3 and AK2 prior to testing. Solid lines represent averages from all experiments and dashed lines represent standard error of the mean. Data in graphs are from N=3 independent experiments where N≥4 block-posts were analyzed per experiment.

SUMMARY OF WORK AND FUTURE DIRECTIONS

Platelets are in charge of sealing wounds in an event of vascular injury to prevent blood loss. This function is carried out by their binding to the exposed vascular matrix at the wound site through the GPIb-IX-V complex, which recognizes the A1 domain of VWF. This bond presents catch bond characteristics: becoming more stable as force is applied to it. Platelets generate cytoskeletal forces and transmit these forces to the surrounding environment to compact and reinforce the hemostatic clot. They use their adhesion receptors such as integrin $\alpha_{IIb}\beta_3$ to transmit these forces to the extracellular environment via their link to the cytoskeleton of the platelet.

Similar to integrin $\alpha_{IIb}\beta_{3,}$ GPIb-IX-V complex is also linked to the actin cytoskeleton. Therefore, we examined the role of the GPIb-IX-V complex in the transmission of these forces to VWF. We used arrays of VWF-coated nanoposts to measure the cytoskeletal forces of single platelets and found that GPIb-IX-V complex transmits a significant proportion of cytoskeletal forces. In particular, we found that these forces are transmitted through the GPIbα subunit of GPIb-IX-V complex as it binds to the A1 domain of VWF at its extracellular side while being linked to the actin cytoskeleton via the scaffold protein filamin A on the intracellular side.

We confirmed our findings using CHO cells that express GPIb-IX complex and then further used them to study the mechanism by which GPIb-IX-V transmits cytoskeletal forces. Using CHO cells that either lacked the filamin A binding site or contained mutations that prevented filamin A binding, we found that, this complex plays a major role in mediating the cytoskeletal force transmission through the GPIb-IX-V complex. However, both CHO cell lines, with either the tail truncation or double mutation, transmitted a significant amount of cytoskeletal force. This may hint to another binding mechanism for filamin A to the cytoplasmic tail of the complex or a second mechanism that associates the complex to the actin cytoskeleton in addition to filamin A such as 14-3-3ξ. Further efforts can be put into investigating these.

The new role identified for GPIb-IX-V complex is an unexpected finding given the widely held notion that platelet forces are transmitted exclusively through integrins. This is the first non-integrin platelet receptor that has is capable of transmitting cytoskeletal forces to

the best of our knowledge. Therefore, the nature and roles that these forces may be playing are still unknown. In a pursuit to investigate the nature of these forces using a myosin activity molecular inhibitor, we found that, the forces transmitted through GPIb-IX-V complex are myosin-dependent and are required to maintain cell attachment through the GPIb-IX-V complex. We think that force transmission may be a compensating mechanism to strengthen the bond through a catch-bond mechanism in the absence of external forces. This finding expands our understanding of how platelets attach to matrices, describing a new mechanism in which catch bonds can be supported by internal forces in the absence of external forces produced by hemodynamic shear forces. These findings may identify a role for GPIb-IX-V complex supporting the adhesion of platelets in arterial regions during hemostasis and thrombosis.

We further studied the role of GPIb-IX-V complex in supporting contractile forces of hemostatic clots that form under flow condition, using a microfluidic device with a multitude of block and micropost pairs at embedded at the bottom of the channel. The study of platelet micro-clots forces revealed that in addition to supporting the formation of the clot at the wound site, GPIb-IX-V complex plays a significant role in supporting the contractile forces of hemostatic clots. Our results indicated that both the GPIb-IX-V complex and integrin $\alpha_{IIb}\beta_3$ are needed for platelet-rich clots to contract.

Together these results identify the first example of a non-integrin receptor that is capable of transmitting forces in platelets. The interruption of the normal interaction between GPIb-IX-V complex and VWF is the basis of a number of blood disorders namely VWF disease. The roles that the forces transmitted through GPIb-IX-V complex may be playing in the context of hemostasis and thrombosis are yet to be determined. The work done here lays down the ground work by identifying a new capability for this bond that can be studied, characterized, and targeted in the future for diagnostic and therapeutic purposes.

REFERENCES

1. Michelson, A.D., *Platelets*. 2nd ed. 2007, Amsterdam ; Boston: Academic Press/Elsevier. xlii, 1343 p.
2. Basmadjian, D., *The effect of flow and mass transport in thrombogenesis.* Ann Biomed Eng, 1990. **18**(6): p. 685-709.
3. Sixma, J.J. and J. Wester, *The hemostatic clot.* Semin Hematol, 1977. **14**(3): p. 265-99.
4. Ruggeri, Z.M. and G.L. Mendolicchio, *Adhesion mechanisms in platelet function.* Circ Res, 2007. **100**(12): p. 1673-85.
5. Andrews, R.K. and M.C. Berndt, *Platelet adhesion: a game of catch and release.* J Clin Invest, 2008. **118**(9): p. 3009-11.
6. Jackson, S.P., W.S. Nesbitt, and E. Westein, *Dynamics of platelet thrombus formation.* J Thromb Haemost, 2009. **7 Suppl 1**: p. 17-20.
7. Kuwahara, M., et al., *Platelet shape changes and adhesion under high shear flow.* Arterioscler Thromb Vasc Biol, 2002. **22**(2): p. 329-34.
8. Peters, C.G., A.D. Michelson, and R. Flaumenhaft, *Granule exocytosis is required for platelet spreading: differential sorting of alpha-granules expressing VAMP-7.* Blood, 2012. **120**(1): p. 199-206.
9. Ruggeri, Z.M., J.A. Dent, and E. Saldivar, *Contribution of distinct adhesive interactions to platelet aggregation in flowing blood.* Blood, 1999. **94**(1): p. 172-8.
10. Maxwell, M.J., et al., *Identification of a 2-stage platelet aggregation process mediating shear-dependent thrombus formation.* Blood, 2007. **109**(2): p. 566-76.
11. Moroi, M. and S.M. Jung, *Integrin-mediated platelet adhesion.* Front Biosci, 1998. **3**: p. d719-28.
12. Mondoro, T.H., M.M. White, and L.K. Jennings, *Active GPIIb-IIIa conformations that link ligand interaction with cytoskeletal reorganization.* Blood, 2000. **96**(7): p. 2487-95.

13. Calaminus, S.D.J., et al., *Myosinlla contractility is required for maintenance of platelet structure during spreading on collagen and contributes to thrombus stability.* Journal of Thrombosis and Haemostasis, 2007. **5**(10): p. 2136-2145.
14. Brass, L.F., L. Zhu, and T.J. Stalker, *Minding the gaps to promote thrombus growth and stability.* J Clin Invest, 2005. **115**(12): p. 3385-92.
15. Basmadjian, D., *The hemodynamic forces acting on thrombi, from incipient attachment of single cells to maturity and embolization.* J Biomech, 1984. **17**(4): p. 287-98.
16. Basmadjian, D., *The hemodynamic and embolizing forces acting on thrombi--II. The effect of pulsatile blood flow.* J Biomech, 1986. **19**(10): p. 837-45.
17. Basmadjian, D., *Embolization: critical thrombus height, shear rates, and pulsatility. Patency of blood vessels.* Journal of Biomedical Materials Research, 1989. **23**(11): p. 1315-26.
18. Boyles, J., et al., *Organization of the Cytoskeleton in Resting, Discoid Platelets - Preservation of Actin-Filaments by a Modified Fixation That Prevents Osmium Damage.* Journal of Cell Biology, 1985. **101**(4): p. 1463-1472.
19. Vicente-Manzanares, M., et al., *Non-muscle myosin II takes centre stage in cell adhesion and migration.* Nat Rev Mol Cell Biol, 2009. **10**(11): p. 778-90.
20. Bischofs, I.B., et al., *Filamentous network mechanics and active contractility determine cell and tissue shape.* Biophys J, 2008. **95**(7): p. 3488-96.
21. Nachmias, V.T., *Cytoskeleton of Human-Platelets at Rest and after Spreading.* Journal of Cell Biology, 1980. **86**(3): p. 795-802.
22. Hartwig, J.H. and M. Desisto, *The Cytoskeleton of the Resting Human Blood-Platelet - Structure of the Membrane Skeleton and Its Attachment to Actin-Filaments.* Journal of Cell Biology, 1991. **112**(3): p. 407-425.
23. Feng, Y.Y. and C.A. Walsh, *The many faces of filamin: A versatile molecular scaffold for cell motility and signalling.* Nature Cell Biology, 2004. **6**(11): p. 1034-1038.
24. Lefebvre, P., et al., *Role of Actin on Platelet-Function - Expression of Fibrinogen Receptor.* Thrombosis and Haemostasis, 1993. **69**(6): p. 698-698.

25. Cohen, I., *The contractile system of blood platelets and its function.* Methods Achiev Exp Pathol, 1979. **9**: p. 40-86.
26. Beckerle, M.C., et al., *Activation-Dependent Redistribution of the Adhesion Plaque Protein, Talin, in Intact Human-Platelets.* Journal of Cell Biology, 1989. **109**(6): p. 3333-3346.
27. Crawford, A.W., J.W. Michelsen, and M.C. Beckerle, *An Interaction between Zyxin and Alpha-Actinin.* Journal of Cell Biology, 1992. **116**(6): p. 1381-1393.
28. Rief, M., et al., *A mechanical unfolding intermediate in an actin-crosslinking protein.* Nature Structural & Molecular Biology, 2004. **11**(1): p. 81-85.
29. Feng, S., X. Lu, and M.H. Kroll, *Filamin A binding stabilizes nascent glycoprotein Ibalpha trafficking and thereby enhances its surface expression.* J Biol Chem, 2005. **280**(8): p. 6709-15.
30. Allingham, J.S., R. Smith, and I. Rayment, *The structural basis of blebbistatin inhibition and specificity for myosin II.* Nature Structural & Molecular Biology, 2005. **12**(4): p. 378-379.
31. Hathaway, D.R. and R.S. Adelstein, *Human platelet myosin light chain kinase requires the calcium-binding protein calmodulin for activity.* Proc Natl Acad Sci U S A, 1979. **76**(4): p. 1653-7.
32. Bouvard, D., et al., *Functional consequences of integrin gene mutations in mice.* Circulation Research, 2001. **89**(3): p. 211-223.
33. Bennett, J.S., *Structure and function of the platelet integrin alpha(IIb)beta(3).* Journal of Clinical Investigation, 2005. **115**(12): p. 3363-3369.
34. Andrews, R.K., et al., *Glycoprotein Ib-IX-V.* Int J Biochem Cell Biol, 2003. **35**(8): p. 1170-4.
35. Lopez, J.A., *The platelet glycoprotein Ib-IX complex.* Blood Coagul Fibrinolysis, 1994. **5**(1): p. 97-119.
36. Hollopeter, G., et al., *Identification of the platelet ADP receptor targeted by antithrombotic drugs.* Nature, 2001. **409**(6817): p. 202-207.
37. Kauskot, A. and M.F. Hoylaerts, *Platelet receptors.* Handb Exp Pharmacol, (210): p. 23-57.

38. Kahn, M.L., *Platelet-collagen responses: molecular basis and therapeutic promise.* Semin Thromb Hemost, 2004. **30**(4): p. 419-25.
39. Andrews, R.K. and M.C. Berndt, *Platelet physiology and thrombosis.* Thromb Res, 2004. **114**(5-6): p. 447-53.
40. Nakamura, F., et al., *The structure of the GPIb-filamin A complex.* Blood, 2006. **107**(5): p. 1925-32.
41. Andrews, R.K., et al., *The glycoprotein Ib-IX-V complex in platelet adhesion and signaling.* Thromb Haemost, 1999. **82**(2): p. 357-64.
42. van der Flier, A. and A. Sonnenberg, *Structural and functional aspects of filamins.* Biochim Biophys Acta, 2001. **1538**(2-3): p. 99-117.
43. Yago, T., et al., *Platelet glycoprotein Ibalpha forms catch bonds with human WT vWF but not with type 2B von Willebrand disease vWF.* J Clin Invest, 2008. **118**(9): p. 3195-207.
44. Feng, S., et al., *Filamin A binding to the cytoplasmic tail of glycoprotein Ibalpha regulates von Willebrand factor-induced platelet activation.* Blood, 2003. **102**(6): p. 2122-9.
45. Ogedegbe, H.O., *An overview of hemostasis.* Laboratory Medicine, 2002. **33**(12): p. 948-953.
46. Nurden, A.T., et al., *Glanzmann thrombasthenia: a review of ITGA2B and ITGB3 defects with emphasis on variants, phenotypic variability, and mouse models.* Blood, 2011. **118**(23): p. 5996-6005.
47. Simon, D., T. Kunicki, and D. Nugent, *Platelet function defects.* Haemophilia, 2008. **14**(6): p. 1240-9.
48. Calvete, J.J., *On the Structure and Function of Platelet Integrin Alpha(Iib)Beta(3), the Fibrinogen Receptor.* Proceedings of the Society for Experimental Biology and Medicine, 1995. **208**(4): p. 346-360.
49. Weiss, H.J., et al., *Decreased adhesion of giant (Bernard-Soulier) platelets to subendothelium. Further implications on the role of the von Willebrand factor in hemostasis.* Am J Med, 1974. **57**(6): p. 920-5.
50. Ruggeri, Z.M., *Mechanisms initiating platelet thrombus formation.* Thromb Haemost, 1997. **78**(1): p. 611-6.

51. Ruggeri, Z.M., et al., *Activation-independent platelet adhesion and aggregation under elevated shear stress.* Blood, 2006. **108**(6): p. 1903-10.
52. Savage, B., F. Almus-Jacobs, and Z.M. Ruggeri, *Specific synergy of multiple substrate-receptor interactions in platelet thrombus formation under flow.* Cell, 1998. **94**(5): p. 657-66.
53. Dopheide, S.M., M.J. Maxwell, and S.P. Jackson, *Shear-dependent tether formation during platelet translocation on von Willebrand factor.* Blood, 2002. **99**(1): p. 159-67.
54. Nesbitt, W.S., et al., *A shear gradient-dependent platelet aggregation mechanism drives thrombus formation.* Nat Med, 2009. **15**(6): p. 665-73.
55. Ono, A., et al., *Identification of a fibrin-independent platelet contractile mechanism regulating primary hemostasis and thrombus growth.* Blood, 2008. **112**(1): p. 90-9.
56. Liang, X.M., et al., *Platelet retraction force measurements using flexible post force sensors.* Lab on a Chip, 2010. **10**(8): p. 991-998.
57. Lam, W.A., et al., *Mechanics and contraction dynamics of single platelets and implications for clot stiffening.* Nat Mater, 2011. **10**(1): p. 61-6.
58. Koteliansky, V.E., et al., *Human plasma fibronectin promotes the adhesion and spreading of platelets on surfaces coated with fibrillar collagen.* FEBS Lett, 1981. **123**(1): p. 59-62.
59. Leytin, V.L., et al., *Time-response changes in the thrombogenicity of platelets spread on a collagen-coated surface.* Thromb Res, 1980. **20**(3): p. 335-41.
60. Frojmovic, M., K. Longmire, and T.G. van de Ven, *Long-range interactions in mammalian platelet aggregation. II. The role of platelet pseudopod number and length.* Biophys J, 1990. **58**(2): p. 309-18.
61. Feuerstein, I.A. and B.D. Ratner, *Adhesion and aggregation of thrombin prestimulated human platelets: evaluation of a series of biomaterials characterized by ESCA.* Biomaterials, 1990. **11**(2): p. 127-32.
62. Sixma, J.J. and P.G. de Groot, *Regulation of platelet adhesion to the vessel wall.* Ann N Y Acad Sci, 1994. **714**: p. 190-9.

63. Eckstein, E.C., et al., *Transport of platelets in flowing blood.* Ann N Y Acad Sci, 1987. **516**: p. 442-52.
64. Yeh, C. and E.C. Eckstein, *Transient lateral transport of platelet-sized particles in flowing blood suspensions.* Biophys J, 1994. **66**(5): p. 1706-16.
65. Spijker, H.T., et al., *On the influence of flow conditions and wettability on blood material interactions.* Biomaterials, 2003. **24**(26): p. 4717-27.
66. de Groot, P.G., I.J. MJ, and J.J. Sixma, *Platelet adhesion to the subendothelium under flow.* Methods Mol Biol, 1999. **96**: p. 159-70.
67. Baumgartner, H.R. and C. Haudenschild, *Adhesion of platelets to subendothelium.* Ann N Y Acad Sci, 1972. **201**: p. 22-36.
68. Anderson, G.H., et al., *Platelet response to shear stress: changes in serotonin uptake, serotonin release, and ADP induced aggregation.* Thromb Res, 1978. **13**(6): p. 1039-47.
69. Weiss, H.J., V.T. Turitto, and H.R. Baumgartner, *Effect of shear rate on platelet interaction with subendothelium in citrated and native blood. I. Shear rate--dependent decrease of adhesion in von Willebrand's disease and the Bernard-Soulier syndrome.* J Lab Clin Med, 1978. **92**(5): p. 750-64.
70. Tschopp, T.B., H.J. Weiss, and H.R. Baumgartner, *Decreased adhesion of platelets to subendothelium in von Willebrand's disease.* J Lab Clin Med, 1974. **83**(2): p. 296-300.
71. Weiss, H.J., T.B. Tschopp, and H.R. Baumgartner, *Impaired interaction (adhesion-aggregation) of platelets with the subendothelium in storage-pool disease and after aspirin ingestion. A comparison with von Willebrand's disease.* N Engl J Med, 1975. **293**(13): p. 619-23.
72. Sakariassen, K.S., et al., *The role of platelet membrane glycoproteins Ib and IIb-IIIa in platelet adherence to human artery subendothelium.* Br J Haematol, 1986. **63**(4): p. 681-91.
73. Badimon, L., et al., *Characterization of a tubular flow chamber for studying platelet interaction with biologic and prosthetic materials: deposition of indium 111-labeled platelets on collagen, subendothelium, and expanded polytetrafluoroethylene.* J Lab Clin Med, 1987. **110**(6): p. 706-18.

74. Roald, H.E., et al., *Initial interactions of platelets and plasma proteins in flowing non-anticoagulated human blood with the artificial surfaces Dacron and PTFE.* Blood Coagul Fibrinolysis, 1994. **5**(3): p. 355-63.
75. Chen, C., et al., *Phosphorylcholine coating of ePTFE reduces platelet deposition and neointimal hyperplasia in arteriovenous grafts.* J Surg Res, 1998. **77**(2): p. 119-25.
76. Hanson, S.R., et al., *Platelet interactions with Dacron vascular grafts. A model of acute thrombosis in baboons.* Arteriosclerosis, 1985. **5**(6): p. 595-603.
77. Cheng, H., et al., *Shear-induced interaction of platelets with von Willebrand factor results in glycoprotein Ibalpha shedding.* Am J Physiol Heart Circ Physiol, 2009. **297**(6): p. H2128-35.
78. Brown, C.H., 3rd, et al., *Morphological, biochemical, and functional changes in human platelets subjected to shear stress.* J Lab Clin Med, 1975. **86**(3): p. 462-71.
79. Giorgio, T.D. and J.D. Hellums, *A cone and plate viscometer for the continuous measurement of blood platelet activation.* Biorheology, 1988. **25**(4): p. 605-24.
80. Furukawa, K., et al., *Real time observation of platelet adhesion to opaque biomaterial surfaces under shear flow conditions.* J Biomed Mater Res, 1999. **46**(1): p. 93-102.
81. Chow, T.W., et al., *Shear stress-induced von Willebrand factor binding to platelet glycoprotein Ib initiates calcium influx associated with aggregation.* Blood, 1992. **80**(1): p. 113-20.
82. Panzer, S., et al., *Loss of high-molecular-weight von Willebrand factor multimers mainly affects platelet aggregation in patients with aortic stenosis.* Thromb Haemost, 2010. **103**(2): p. 408-14.
83. Yin, W., S.K. Shanmugavelayudam, and D.A. Rubenstein, *The effect of physiologically relevant dynamic shear stress on platelet and endothelial cell activation.* Thromb Res, 2011. **127**(3): p. 235-41.
84. Furukawa, K.S., et al., *Quantitative analysis of human platelet adhesions under a small-scale flow device.* Artif Organs, 2010. **34**(4): p. 295-300.

85. Sakariassen, K.S., et al., *A perfusion chamber developed to investigate platelet interaction in flowing blood with human vessel wall cells, their extracellular matrix, and purified components.* J Lab Clin Med, 1983. **102**(4): p. 522-35.
86. Hubbell, J.A. and L.V. McIntire, *Visualization and analysis of mural thrombogenesis on collagen, polyurethane and nylon.* Biomaterials, 1986. **7**(5): p. 354-63.
87. Sakariassen, K.S., et al., *Growth and stability of thrombi in flowing citrated blood: assessment of platelet-surface interactions with computer-assisted morphometry.* Thromb Haemost, 1988. **60**(3): p. 392-8.
88. Savage, B., E. Saldivar, and Z.M. Ruggeri, *Initiation of platelet adhesion by arrest onto fibrinogen or translocation on von Willebrand factor.* Cell, 1996. **84**(2): p. 289-97.
89. van Breugel, H.H., J.J. Sixma, and R.M. Heethaar, *Effects of flow pulsatility on platelet adhesion to subendothelium.* Arteriosclerosis, 1988. **8**(3): p. 332-5.
90. Barstad, R.M., P. Kierulf, and K.S. Sakariassen, *Collagen induced thrombus formation at the apex of eccentric stenoses--a time course study with non-anticoagulated human blood.* Thromb Haemost, 1996. **75**(4): p. 685-92.
91. de Graaf, J.C., et al., *Nitric oxide functions as an inhibitor of platelet adhesion under flow conditions.* Circulation, 1992. **85**(6): p. 2284-90.
92. Roux, S.P., et al., *Effect of aspirin and epinephrine on experimentally induced thrombogenesis in dogs. A parallelism between in vivo and ex vivo thrombosis models.* Arterioscler Thromb, 1991. **11**(5): p. 1182-91.
93. Maxwell, M.J., et al., *Shear induces a unique series of morphological changes in translocating platelets: effects of morphology on translocation dynamics.* Arterioscler Thromb Vasc Biol, 2006. **26**(3): p. 663-9.
94. Sakariassen, K.S., P.A. Bolhuis, and J.J. Sixma, *Human blood platelet adhesion to artery subendothelium is mediated by factor VIII-Von Willebrand factor bound to the subendothelium.* Nature, 1979. **279**(5714): p. 636-8.
95. Kirchhofer, D., T.B. Tschopp, and H.R. Baumgartner, *Active site-blocked factors VIIa and IXa differentially inhibit fibrin formation in a human ex vivo thrombosis model.* Arterioscler Thromb Vasc Biol, 1995. **15**(8): p. 1098-106.

96. Sixma, J.J., et al., *A new perfusion chamber to detect platelet adhesion using a small volume of blood.* Thromb Res, 1998. **92**(6 Suppl 2): p. S43-6.
97. Xia, Y.N. and G.M. Whitesides, *Soft lithography.* Angewandte Chemie-International Edition, 1998. **37**(5): p. 551-575.
98. Duffy, D.C., et al., *Rapid prototyping of microfluidic systems in poly(dimethylsiloxane).* Analytical Chemistry, 1998. **70**(23): p. 4974-4984.
99. Whitesides, G.M., et al., *Soft lithography in biology and biochemistry.* Annu Rev Biomed Eng, 2001. **3**: p. 335-73.
100. van der Meer, A.D., et al., *Microfluidic Technology in Vascular Research.* Journal of Biomedicine and Biotechnology, 2009.
101. Prabhakarpandian, B., et al., *Microfluidic devices for modeling cell-cell and particle-cell interactions in the microvasculature.* Microvasc Res, 2011. **82**(3): p. 210-20.
102. Remijn, J.A., et al., *Absence of fibrinogen in afibrinogenemia results in large but loosely packed thrombi under flow conditions.* Thromb Haemost, 2001. **85**(4): p. 736-42.
103. Tsuji, S., et al., *Real-time analysis of mural thrombus formation in various platelet aggregation disorders: distinct shear-dependent roles of platelet receptors and adhesive proteins under flow.* Blood, 1999. **94**(3): p. 968-75.
104. Neeves, K.B. and S.L. Diamond, *A membrane-based microfluidic device for controlling the flux of platelet agonists into flowing blood.* Lab Chip, 2008. **8**(5): p. 701-9.
105. Conant, C.G., et al., *Using well-plate microfluidic devices to conduct shear-based thrombosis assays.* J Lab Autom, 2011. **16**(2): p. 148-52.
106. Tovar-Lopez, F.J., et al., *A microfluidics device to monitor platelet aggregation dynamics in response to strain rate micro-gradients in flowing blood.* Lab Chip, 2010. **10**(3): p. 291-302.
107. Hoff, J., *Methods of blood collection in the mouse.* Lab Animal, 2000. **29**(10): p. 47-53.

108. Neeves, K.B., et al., *Microfluidic focal thrombosis model for measuring murine platelet deposition and stability: PAR4 signaling enhances shear-resistance of platelet aggregates.* J Thromb Haemost, 2008. **6**(12): p. 2193-201.
109. Kent, N.J., et al., *Shear-mediated platelet adhesion analysis in less than 100 mul of blood: toward a POC platelet diagnostic.* IEEE Trans Biomed Eng, 2011. **58**(3): p. 826-30.
110. Stolla, M., et al., *The kinetics of alphaIIbbeta3 activation determines the size and stability of thrombi in mice: implications for antiplatelet therapy.* Blood, 2011. **117**(3): p. 1005-13.
111. Wannemacher, K.M., et al., *Diminished contact-dependent reinforcement of Syk activation underlies impaired thrombus growth in mice lacking Semaphorin 4D.* Blood, 2010. **116**(25): p. 5707-15.
112. Gutierrez, E., et al., *Microfluidic devices for studies of shear-dependent platelet adhesion.* Lab Chip, 2008. **8**(9): p. 1486-95.
113. Conant, C.G., et al., *Well plate microfluidic system for investigation of dynamic platelet behavior under variable shear loads.* Biotechnol Bioeng, 2011.
114. Colace, T., et al., *Analysis of morphology of platelet aggregates formed on collagen under laminar blood flow.* Ann Biomed Eng, 2011. **39**(2): p. 922-9.
115. Maloney, S.F., L.F. Brass, and S.L. Diamond, *P2Y12 or P2Y1 inhibitors reduce platelet deposition in a microfluidic model of thrombosis while apyrase lacks efficacy under flow conditions.* Integr Biol (Camb), 2010. **2**(4): p. 183-92.
116. Geiger, B., et al., *Transmembrane extracellular matrix--cytoskeleton crosstalk.* Nat Rev Mol Cell Biol, 2001. **2**(11): p. 793-805.
117. Thomas, S.G., et al., *Studies on the actin-binding protein HS1 in platelets.* BMC Cell Biol, 2007. **8**: p. 46.
118. Law, D.A., et al., *Integrin cytoplasmic tyrosine motif is required for outside-in alphaIIbbeta3 signalling and platelet function.* Nature, 1999. **401**(6755): p. 808-11.
119. Suzuki-Inoue, K., et al., *Involvement of Src kinases and PLCgamma2 in clot retraction.* Thromb Res, 2007. **120**(2): p. 251-8.

120. Katori, N., et al., *The effects of platelet count on clot retraction and tissue plasminogen activator-induced fibrinolysis on thrombelastography.* Anesth Analg, 2005. **100**(6): p. 1781-5.
121. Levrat, A., et al., *Evaluation of rotation thrombelastography for the diagnosis of hyperfibrinolysis in trauma patients.* Br J Anaesth, 2008. **100**(6): p. 792-7.
122. Rugeri, L., et al., *Diagnosis of early coagulation abnormalities in trauma patients by rotation thrombelastography.* J Thromb Haemost, 2007. **5**(2): p. 289-95.
123. Carroll, R.C., et al., *Early evaluation of acute traumatic coagulopathy by thrombelastography.* Transl Res, 2009. **154**(1): p. 34-9.
124. Haenecke, P. and M. Klouche, *Thrombelastography today: Practicability and analytical power.* Transfusion Medicine and Hemotherapy, 2007. **34**(6): p. 421-428.
125. Cohen, I. and A. De Vries, *Platelet contractile regulation in an isometric system.* Nature, 1973. **246**(5427): p. 36-7.
126. Salganicoff, L., et al., *The platelet strip. I. A low-fibrin contractile model of thrombin-activated platelets.* Am J Physiol, 1985. **249**(3 Pt 1): p. C279-87.
127. Salganicoff, L. and R.W. Sevy, *The platelet strip. II. Pharmacomechanical coupling in thrombin-activated human platelets.* Am J Physiol, 1985. **249**(3 Pt 1): p. C288-96.
128. Cohen, I., D.L. Burk, and J.G. White, *The effect of peptides and monoclonal antibodies that bind to platelet glycoprotein IIb-IIIa complex on the development of clot tension.* Blood, 1989. **73**(7): p. 1880-7.
129. Carr, M.E., Jr. and S.L. Zekert, *Measurement of platelet-mediated force development during plasma clot formation.* Am J Med Sci, 1991. **302**(1): p. 13-8.
130. Carr, M.E., Jr., *Development of platelet contractile force as a research and clinical measure of platelet function.* Cell Biochem Biophys, 2003. **38**(1): p. 55-78.
131. Carr, M.E., Jr., et al., *Effect of non-heparin thrombin antagonists on thrombin generation, platelet function, and clot structure in whole blood.* Cell Biochem Biophys, 2003. **39**(2): p. 89-99.

132. Carr, M.E., Jr., et al., *Enhanced platelet force development despite drug-induced inhibition of platelet aggregation in patients with thromboangiitis obliterans--two case reports.* Vasc Endovascular Surg, 2002. **36**(6): p. 473-80.
133. Greilich, P.E., et al., *Reductions in platelet force development by cardiopulmonary bypass are associated with hemorrhage.* Anesth Analg, 1995. **80**(3): p. 459-65.
134. Brophy, D.F., et al., *The effect of uremia on platelet contractile force, clot elastic modulus and bleeding time in hemodialysis patients.* Thromb Res, 2007. **119**(6): p. 723-9.
135. Brophy, D.F., et al., *Antifactor Xa activity correlates to thrombin generation time, platelet contractile force and clot elastic modulus following ex vivo enoxaparin exposure in patients with and without renal dysfunction.* J Thromb Haemost, 2004. **2**(8): p. 1299-304.
136. Carr, M.E., Jr., et al., *Batroxobin-induced clots exhibit delayed and reduced platelet contractile force in some patients with clotting factor deficiencies.* J Thromb Haemost, 2003. **1**(2): p. 243-9.
137. Carr, M.E., Jr., et al., *Aprotinin counteracts heparin-induced inhibition of platelet contractile force.* Thromb Res, 2002. **108**(2-3): p. 161-8.
138. Krishnaswami, A., et al., *Patients with coronary artery disease who present with chest pain have significantly elevated platelet contractile force and clot elastic modulus.* Thromb Haemost, 2002. **88**(5): p. 739-44.
139. Carr, M.E., Jr., E.J. Martin, and S.L. Carr, *Delayed, reduced or inhibited thrombin production reduces platelet contractile force and results in weaker clot formation.* Blood Coagul Fibrinolysis, 2002. **13**(3): p. 193-7.
140. Tan, J.L., et al., *Cells lying on a bed of microneedles: an approach to isolate mechanical force.* Proc Natl Acad Sci U S A, 2003. **100**(4): p. 1484-9.
141. du Roure, O., et al., *Force mapping in epithelial cell migration.* Proc Natl Acad Sci U S A, 2005. **102**(7): p. 2390-5.
142. Pirone, D.M., et al., *An inhibitory role for FAK in regulating proliferation: a link between limited adhesion and RhoA-ROCK signaling.* J Cell Biol, 2006. **174**(2): p. 277-88.

143. Fu, J., et al., *Mechanical regulation of cell function with geometrically modulated elastomeric substrates.* Nat Methods, 2010. **7**(9): p. 733-6.
144. Saez, A., et al., *Is the mechanical activity of epithelial cells controlled by deformations or forces?* Biophys J, 2005. **89**(6): p. L52-4.
145. Sniadecki, N.J., et al., *Magnetic microposts for mechanical stimulation of biological cells: fabrication, characterization, and analysis.* Rev Sci Instrum, 2008. **79**(4): p. 044302.
146. Chen, C.S., M.T. Yang, and N.J. Sniadecki, *Geometric considerations of micro- to nanoscale elastomeric post arrays to study cellular traction forces.* Advanced Materials, 2007. **19**(20): p. 3119-+.
147. Cai, Y., et al., *Nonmuscle myosin IIA-dependent force inhibits cell spreading and drives F-actin flow.* Biophys J, 2006. **91**(10): p. 3907-20.
148. Liu, Z., N.J. Sniadecki, and C.S. Chen, *Mechanical Forces in Endothelial Cells during Firm Adhesion and Early Transmigration of Human Monocytes.* Cell Mol Bioeng, 2010. **3**(1): p. 50-59.
149. Rabodzey, A., et al., *Mechanical forces induced by the transendothelial migration of human neutrophils.* Biophys J, 2008. **95**(3): p. 1428-38.
150. Nelson, C.M., et al., *Emergent patterns of growth controlled by multicellular form and mechanics.* Proc Natl Acad Sci U S A, 2005. **102**(33): p. 11594-11599.
151. Ruiz, S.A. and C.S. Chen, *Emergence of patterned stem cell differentiation within multicellular structures.* Stem Cells, 2008. **26**(11): p. 2921-7.
152. Kajzar, A., et al., *Toward physiological conditions for cell analyses: forces of heart muscle cells suspended between elastic micropillars.* Biophys J, 2008. **94**(5): p. 1854-66.
153. Liu, Z., et al., *Mechanical tugging force regulates the size of cell-cell junctions.* Proc Natl Acad Sci U S A, 2010. **107**(22): p. 9944-9.
154. Maruthamuthu, V., et al., *Cell-ECM traction force modulates endogenous tension at cell-cell contacts.* Proc Natl Acad Sci U S A, 2011. **108**(12): p. 4708-13.
155. Ghibaudo, M., et al., *Traction forces and rigidity sensing regulate cell functions.* Soft Matter, 2008. **4**(9): p. 1836-1843.

156. Sniadecki, N.J., et al., *Magnetic microposts as an approach to apply forces to living cells.* Proc Natl Acad Sci U S A, 2007. **104**(37): p. 14553-8.
157. Lemmon, C.A., et al., *Shear force at the cell-matrix interface: enhanced analysis for microfabricated post array detectors.* Mech Chem Biosyst, 2005. **2**(1): p. 1-16.
158. Kim, K., et al., *Calibrated micropost arrays for biomechanical characterisation of cardiomyocytes.* Micro & Nano Letters, 2011. **6**(5): p. 317-322.
159. Zhao, Y. and X. Zhang, *Cellular mechanics study in cardiac myocytes using PDMS pillars array.* Sensors and Actuators a-Physical, 2006. **125**(2): p. 398-404.
160. Yang, M.T., et al., *Assaying stem cell mechanobiology on microfabricated elastomeric substrates with geometrically modulated rigidity.* Nat Protoc, 2011. **6**(2): p. 187-213.
161. Scheuring, S., I. Casuso, and F. Rico, *Biological AFM: where we come from - where we are - where we may go.* Journal of Molecular Recognition, 2011. **24**(3): p. 406-413.
162. Radmacher, M., *Measuring the elastic properties of biological samples with the AFM.* Ieee Engineering in Medicine and Biology Magazine, 1997. **16**(2): p. 47-57.
163. Rotsch, C. and M. Radmacher, *Drug-induced changes of cytoskeletal structure and mechanics in fibroblasts: An atomic force microscopy study.* Biophysical Journal, 2000. **78**(1): p. 520-535.
164. Mathur, A.B., et al., *Endothelial, cardiac muscle and skeletal muscle exhibit different viscous and elastic properties as determined by atomic force microscopy.* Journal of Biomechanics, 2001. **34**(12): p. 1545-1553.
165. Alcaraz, J., et al., *Microrheology of human lung epithelial cells measured by atomic force microscopy.* Biophys J, 2003. **84**(3): p. 2071-9.
166. Laurent, V.M., et al., *Gradient of rigidity in the lamellipodia of migrating cells revealed by atomic force microscopy.* Biophys J, 2005. **89**(1): p. 667-75.
167. Solon, J., et al., *Fibroblast adaptation and stiffness matching to soft elastic substrates.* Biophysical Journal, 2007. **93**(12): p. 4453-4461.

168. Maloney, J.M., et al., *Mesenchymal stem cell mechanics from the attached to the suspended state.* Biophys J, 2010. **99**(8): p. 2479-87.
169. Cross, S.E., et al., *Nanomechanical analysis of cells from cancer patients.* Nat Nanotechnol, 2007. **2**(12): p. 780-3.
170. Benoit, M., et al., *Discrete interactions in cell adhesion measured by single-molecule force spectroscopy.* Nature Cell Biology, 2000. **2**(6): p. 313-317.
171. Helenius, J., et al., *Single-cell force spectroscopy.* Journal of Cell Science, 2008. **121**(11): p. 1785-1791.
172. Puech, P.H., et al., *A new technical approach to quantify cell-cell adhesion forces by AFM.* Ultramicroscopy, 2006. **106**(8-9): p. 637-44.
173. Moy, V.T., X.H. Zhang, and E. Wojcikiewicz, *Force spectroscopy of the leukocyte function-associated antigen-1/intercellular adhesion molecule-1 interaction.* Biophysical Journal, 2002. **83**(4): p. 2270-2279.
174. Wojcikiewicz, E.P., et al., *Force spectroscopy of LFA-1 and its ligands, ICAM-1 and ICAM-2.* Biomacromolecules, 2006. **7**(11): p. 3188-3195.
175. Sokurenko, E.V., V. Vogel, and W.E. Thomas, *Catch-bond mechanism of force-enhanced adhesion: counterintuitive, elusive, but ... widespread?* Cell Host Microbe, 2008. **4**(4): p. 314-23.
176. Zhu, C., et al., *Demonstration of catch bonds between an integrin and its ligand.* Journal of Cell Biology, 2009. **185**(7): p. 1275-1284.
177. Zhu, C., et al., *Force history dependence of receptor-ligand dissociation.* Biophysical Journal, 2005. **88**(2): p. 1458-1466.
178. Khurana, S., et al., *Monitoring platelet glycoprotein IIb/IIIa-fibrin interaction with tissue factor-activated thromboelastography.* J Lab Clin Med, 1997. **130**(4): p. 401-11.
179. Reininger, C.B., et al., *Quantitative analysis of platelet function using stagnation point flow aggregometry. First clinical results.* Int Angiol, 1992. **11**(4): p. 247-55.
180. Schwarz Henriques, S., et al., *Force field evolution during human blood platelet activation.* J Cell Sci. **125**(Pt 16): p. 3914-20.
181. Sniadecki, N.J. and C.S. Chen, *Microfabricated Silicone Elastomeric Post Arrays for Measuring Traction Forces of Adherent Cells*, in *Methods in Cell Biology:*

Cell Mechanics, Y. Wang and D.E. Discher, Editors. 2007, Elsevier Inc.: San Diego, CA. p. 313-328.

182. Ruggeri, Z.M., *The role of von Willebrand factor in thrombus formation.* Thromb Res, 2007. **120 Suppl 1**: p. S5-9.
183. Lopez, J.A., et al., *Efficient plasma membrane expression of a functional platelet glycoprotein Ib-IX complex requires the presence of its three subunits.* J Biol Chem, 1992. **267**(18): p. 12851-9.
184. Cranmer, S.L., et al., *Identification of a unique filamin A binding region within the cytoplasmic domain of glycoprotein Ibalpha.* Biochem J, 2005. **387**(Pt 3): p. 849-58.
185. Chen, Y., et al., *The abnormal proplatelet formation in MYH9-related macrothrombocytopenia results from an increased actomyosin contractility and is rescued by myosin IIA inhibition.* J Thromb Haemost, 2013. **11**(12): p. 2163-75.
186. Shin, J.W., et al., *Myosin-II inhibition and soft 2D matrix maximize multinucleation and cellular projections typical of platelet-producing megakaryocytes.* Proc Natl Acad Sci U S A, 2011. **108**(28): p. 11458-63.
187. Chen, J. and J.A. Lopez, *Interactions of platelets with subendothelium and endothelium.* Microcirculation, 2005. **12**(3): p. 235-46.
188. Boon, G.D., *An overview of hemostasis.* Toxicol Pathol, 1993. **21**(2): p. 170-9.
189. Alevriadou, B.R., et al., *Real-Time Analysis of Shear-Dependent Thrombus Formation and Its Blockade by Inhibitors of Vonwillebrand-Factor Binding to Platelets.* Blood, 1993. **81**(5): p. 1263-1276.
190. Back, L.D., J.R. Radbill, and D.W. Crawford, *Analysis of pulsatile, viscous blood flow through diseased coronary arteries of man.* J Biomech, 1977. **10**(5-6): p. 339-53.
191. Reininger, A.J., et al., *Mechanism of platelet adhesion to von Willebrand factor and microparticle formation under high shear stress.* Blood, 2006. **107**(9): p. 3537-45.
192. Strony, J., et al., *Analysis of shear stress and hemodynamic factors in a model of coronary artery stenosis and thrombosis.* Am J Physiol, 1993. **265**(5 Pt 2): p. H1787-96.

193. Mailhac, A., et al., *Effect of an eccentric severe stenosis on fibrin(ogen) deposition on severely damaged vessel wall in arterial thrombosis. Relative contribution of fibrin(ogen) and platelets.* Circulation, 1994. **90**(2): p. 988-96.